A rapid application emissions-to-impacts tool for scenario assessment: Probabilistic Regional Impacts from Model patterns and Emissions (PRIME)

Camilla Mathison[1,3], Eleanor J. Burke[1], Gregory Munday[1], Chris D. Jones[1,7], Chris J Smith[3,4], Norman J. Steinert[5], Andy J Wiltshire[1,6], Chris Huntingford[2], Eszter Kovacs[3], Laila K. Gohar[1], Rebecca M. Varney[6], and Douglas McNeall[1,6]

[1]Met Office Hadley Centre, Exeter, UK
[2]UK Centre for Ecology and Hydrology, Wallingford, UK
[3]University of Leeds, Leeds, UK
[4]International Institute for Applied Systems Analysis (IIASA), Laxenburg, Austria
[5]NORCE Norwegian Research Centre, Bjerknes Centre for Climate Research, Bergen, Norway
[6]Faculty of Environment, Science and Economy, University of Exeter, Exeter, UK
[7]School of Geographical Sciences, University of Bristol, Bristol, UK

Correspondence: Camilla Mathison (camilla.mathison@metoffice.gov.uk)

Abstract.

Climate policies evolve quickly, and new scenarios designed around these policies are used to illustrate how they impact global mean temperatures using simple climate models (or climate emulators). Simple climate models are extremely efficient although limited to showing only the global picture. Within the Intergovernmental Panel on Climate Change (IPCC) framework understanding of the regional impacts of scenarios that include the most recent science is needed to provide general information to society and allow targeted policy decisions to be made quickly. To address this, we present PRIME (Probabilistic Regional Impacts from Model patterns and Emissions), a new flexible probabilistic framework which aims to provide an efficient mechanism to run new scenarios without the significant overheads of larger more complex Earth system models (ESMs). PRIME provides the capability to include features of the most recent ESM projections, science, and scenarios to run ensemble simulations on multi-centennial timescales and include analysis of many key variables that are relevant and important for impacts assessments. We use a simple climate model to provide the global temperature response to emissions scenarios. These estimated temperatures are used to scale monthly-mean patterns from a large number of CMIP6 ESMs. These patterns provide the inputs to a "weather generator" algorithm and a land-surface model. The PRIME system thus generates an end-to-end estimate of the land-surface impacts from the emissions scenarios. We test PRIME using known scenarios in the form of the Shared Socioeconomic Pathways (SSPs), to demonstrate that our model reproduces the ESM climate responses to these scenarios. We show results for a range of scenarios: the SSP5-8.5 high emissions scenario was used to define the patterns. SSP1-2.6, a mitigation scenario with low emissions and SSP5-3.4-OS, an overshoot scenario were used as verification data. PRIME correctly represents the climate response (and spread) for these known scenarios, which gives us confidence our simulation framework will be useful for rapidly providing probabilistic spatially resolved information for novel climate scenarios, thereby substantially reducing the time between new scenarios being released and the availability of regional impacts information.

1 Introduction

A major gap currently exists in our capability to rapidly assess and predict regional impacts of climate change in response to novel future pathways of climate change and rapidly evolving policies. Sophisticated and specialist climate impacts models exist that assess the regional implications of future climate scenarios for a range of impacts sectors, such as: crops, biomes, water, fire and permafrost, for example through the Inter-Sectoral Impacts Model Intercomparison Project (ISIMIP; Frieler et al., 2017; Warszawski et al., 2014, 2013). ISIMIP provides a consistent framework for assessing climate impacts using a large ensemble of models across a range of sectors. However, impact models are often specific to particular sectors and are in themselves complicated to set up. Usually, their use occurs at the end of a long chain of events: commencing with generation of emissions scenarios, running one or more Earth system models (ESMs), potentially bias-correcting ESM output, then finally running the impact model.

In order to assess impacts resulting from climate change more systematically, ISIMIP provides output of ESMs to impact modellers. But even then, there is a long delay from creation of the scenarios to our ability to assess their impacts. For example, the most recent impacts assessment of the Intergovernmental Panel on Climate Change (IPCC), the Sixth Assessment Report (AR6) Working Group II (Climate Change Impacts, Adaptation and Vulnerability: WGII) (Pörtner et al., 2022), relies heavily on literature based on impacts studies using output from the previous generation of the Coupled Model Intercomparison Project (CMIP5), rather than the most recent CMIP6 used in AR6 Working Group I (IPCC, 2021). This means that both the scenarios (RCPs; van Vuuren et al., 2011) and climate models themselves (e.g., HadGEM2-ES Jones et al., 2011; Collins et al., 2011) used to assess climate impacts by the IPCC are at least a decade old.

This apparent bottleneck is caused by the significant issue that ESMs, which are the main mechanism for projecting future climate change, are computationally demanding, so only a limited number of simulations may be performed. As ESMs take years to develop, test, and run, scenarios of future climate change are only produced periodically on a timeframe designed to align with IPCC assessment reports, such as contributions to the CMIP phases (Taylor et al., 2012; Eyring et al., 2016). Nevertheless, ESMs remain the best tools for understanding mechanisms of climate change, and regional climate projections could not be performed without them.

One popular method to enable projections of future climate change for novel emissions scenarios, and yet capture the process understanding implicit in the ESMs simulations that do exist, is via "pattern-scaling" (Zelazowski et al., 2018; James et al., 2017; Huntingford et al., 2010; Mitchell, 2003). Such scaling assumes that local and monthly changes in near-surface meteorological conditions correlate linearly with the level of global warming. Lee et al. (2021) note that pattern scaling has known limitations, for example having lower skill for variables with large spatial variability (Herger et al., 2015; Tebaldi and

Arblaster, 2014), or when attempting to recreate moving boundaries such as sea ice extent and snow cover (Collins et al., 2013). Nonetheless, the benefits of pattern scaling to enable rapid reconstruction of spatial patterns based on global temperature make it an extremely valuable tool for studying, for example, carbon cycle feedbacks using an intermediate complexity climate model (Mercado et al., 2009; Burke et al., 2017).

Other tools are currently being developed to explore the use of pattern scaling for local climate change impacts. The Modular Earth System Model Emulator with spatially resolved output (MESMER; Beusch et al. (2020)) draws on patterns of temperature from CMIP6 models and its extension to this (MESMER-M; Nath et al., 2022) focuses on spatially resolved monthly temperature or extremes (MESMER-X; Quilcaille et al., 2022). MESMER is an emulator of temperature patterns and uses a stochastic representation of natural variability. Goodwin et al. (2020) have also used pattern scaling with the WASP global emulator to look at local temperature projections. Alternatively, the STITCHES system (Tebaldi et al., 2022) presents an option for ESM emulation for impacts research by 'stitching' together ESM output from known scenarios.

Using pattern-scaled climate variables instead of ESM output to drive impacts models therefore offers a useful opportunity to more quickly derive impacts information from new scenarios. This does not imply that this type of input should replace ESMs or ISIMIP bias-corrected data, but provide a steer on which scenarios it would be most useful for ESMs to run or which ones to bias-correct for use in more specialist impacts models. Global mean temperature is readily and efficiently calculated from emissions scenarios using one of a range of climate emulators (Nicholls et al., 2020), which are computationally cheap to run. The regional climate patterns are then scaled by applying global mean temperatures produced from emulators. The ability to run simulations without running the full ESM is particularly useful for assessing novel scenarios, particularly those that are regularly updated (Richters et al., 2022) to address specific questions around Paris agreement compliance and overshoot (Rogelj et al., 2018; IPCC, 2022), or to answer "what-if" questions relating to the Earth's geophysical response (Dvorak et al., 2022). These scenarios may never be run through full ESMs because of the vast compute resources required, but understanding their regional impacts may be important in answering adaptation and mitigation questions. The efficiency and flexibility of emulators allows them to run ensembles in a probabilistic Monte Carlo framework, spanning the range of assessed climate uncertainty with different parameter choices (Nicholls et al., 2021). We propose that these emulator systems provide an important and relatively (computationally) cheap first look at new scenarios that could inform future ESM developments.

Here we present PRIME (Probabilistic Regional Impacts from Model patterns and Emissions): a framework designed to bridge the gap between scenarios and impacts in a computationally efficient manner. PRIME builds on previous work of Huntingford and Cox (2000) which culminated in the formal coupling of the analogue model (i.e. Energy Balance Model or EBM plus climate patterns) to a vegetation model that created the modelling framework called IMOGEN (Integrated Model Of Global Effects of climatic aNomalies) (Huntingford et al., 2010). IMOGEN also contains a simple single box representation of the oceanic drawdown of atmospheric carbon dioxide as a function of global mean temperature change over the oceans and CO_2 level. As such, IMOGEN contains a global carbon cycle, and so instead may be forced by CO_2 emissions, and from this by accounting for land-atmosphere and land-ocean interactions, atmospheric CO_2 levels are projected. IMOGEN was originally calibrated against ESMs in the Coupled Model Intercomparison Project version 3 (CMIP3) (Zelazowski et al., 2018) and later against version 5 (CMIP5). In this paper we replace the EBM in IMOGEN with the FaIR model, which means we can

extend beyond the influence of CO_2 and consider other greenhouse gases and short-lived climate forcers that also influence the global temperature. Using FaIR also brings in the latest science from the reduced complexity modelling community. While the underlying IMOGEN model remains inspired by and based largely on the code in IMOGEN (Huntingford and Cox, 2000), in PRIME we update the patterns to use those from CMIP6 models and couple the output from IMOGEN to a full land surface model to study land-based impacts.

In this way, PRIME facilitates faster pull-through of state-of-the-art science from the latest scenarios and regional climate change patterns (from the latest ESMs) all the way to the simulation of regional impacts. PRIME includes the latest understanding of climate and carbon cycle feedbacks, the latest spatial patterns of climate change, and a leading land-surface model/impacts model. In PRIME we accommodate a broad range of variables in addition to temperature, with a focus on those which are important for impacts assessments. PRIME is a flexible framework, with the choices made by the user affecting the way that ensemble members and patterns are selected. However, a Rose suite to simplify running the PRIME framework using the choices presented here is in development. The elements of PRIME are explained in more detail in Section 2. An evaluation of the performance of the framework is provided in Section 3, additional results that are relevant for impacts applications are presented in Section 4, with discussion and conclusions in Section 5.

2 Methods

PRIME is a rapid-response tool designed to explore spatially resolved climate and impacts of scenarios as soon as they are developed. It draws on comprehensive CMIP multi-model ensemble results, but extends these to fill gaps not yet populated by ESMs or impact models and can extend simulations into the future to simulate multi-century response. PRIME produces probabilistic sampling of a range of uncertainties, including global climate and carbon cycle sensitivity and spatial patterns of climate change. It opens the potential to also span perturbed parameter uncertainty in land and impacts models and provides the ability to propagate constraints onto impacts projections through either prior constraint on parameters or posterior selection of ensemble members.

Figure 1 shows the components that make up the PRIME framework. The starting point is emissions scenarios such as from integrated assessment models (IAMs), which are used to drive the global climate emulator FaIRv1.6.2 (Smith et al., 2018, see Sect. 2.1). FaIR can probabilistically sample uncertainty in climate and carbon cycle response to emissions. Its global mean temperature projections are then used to reconstruct the regional climate change for a number of climate variables using the patterns derived from ESMs (see Sect. 2.2). These regional patterns, along with CO_2 concentrations from FaIR, are used to drive the JULES land surface model, from which various climate impacts can be derived.

2.1 Emulator of Global Temperature change

The Finite-amplitude Impulse Response (FaIR) model is a climate emulator that takes inputs of greenhouse gas and short-lived climate forcer emissions and produces projections of global mean surface temperature (Smith et al., 2018; Leach et al., 2021). FaIR calculates greenhouse gas concentrations (including CO_2) and effective radiative forcing as intermediate steps. FaIR

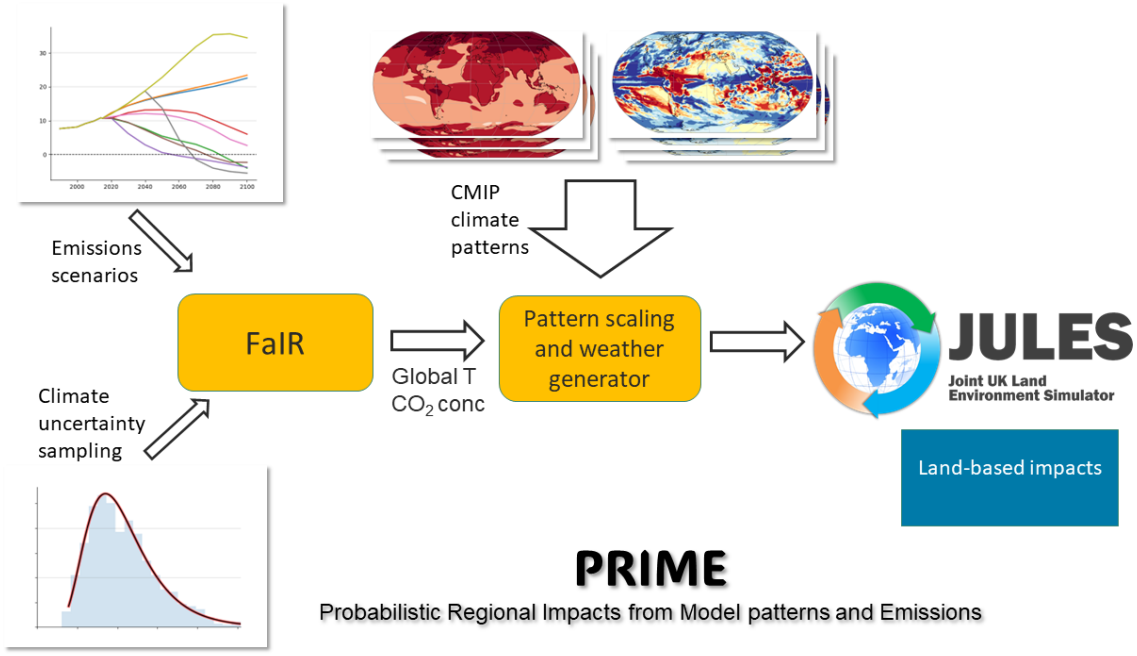

Figure 1. Schematic of the PRIME framework. Emissions scenarios provide input in terms of emissions of CO_2, other greenhouse gases, and aerosols and can be taken from IAMs or idealised experiments. The FaIR climate emulator samples uncertainty from the climate and carbon cycle response to emissions and outputs global temperature and CO_2 concentration. PRIME then scales patterns of climate change from CMIP climate models by the global temperature and uses a weather generator to downscale these to sub-daily driving data for the JULES land surface model. JULES outputs a broad range of land-based impacts-relevant quantities such as gross primary productivity (GPP), Net primary productivity (NPP), vegetation cover, soil moisture and runoff.

contains modules that simulate the carbon cycle feedback (changes in uptake of CO_2 by land and ocean sinks with increasing CO_2 emissions and warming), and forcing from aerosols, ozone, land-use change and several other categories of anthropogenic and natural forcings. These relationships in FaIR are designed to capture the large-scale behaviour of complex Earth system models, and are governed by a number of tuneable parameters.

As part of the IPCC AR6 Working Group 1 (The Physical Science Basis of Climate Change: WGI; IPCC, 2021), a 1.6 million member prior ensemble of FaIR v1.6.2 was produced. This large ensemble is reduced using the historical temperature record to eliminate those members with a large error, with the aim of reproducing the uncertainty range in present day relative to the Pre-Industrial. Through simultaneously constraining on several observable and emergent climate metrics including Equilibrium Climate sensitivity (ECS), Transient Climate Response (TCR), Aerosol, CO_2 concentration, and ocean heat change, the ensemble is reduced to the 2237 members used in AR6 (Forster et al., 2021; Smith et al., 2021, 2023). This ensemble of 2237 parameter sets was taken forward and used for assessing emissions pathways derived from IAMs in the Working Group III (Mitigation of Climate Change: WGIII) report (Riahi et al., 2022). We use this ensemble (Smith, 2022) as part of the PRIME

framework, this AR6 calibration is described in detail in fair-calibrate V1.4.0 (Smith et al., 2024). The climate uncertainty parameters sampled include radiative forcing from different drivers (including aerosols), carbon cycle sensitivities, timescales of climate response to forcing, and climate sensitivity. In this study, to make the ensemble size manageable, we reduce the total number of ensemble members by sub-sampling from within the 2237 parameter sets to explore the full range of global temperature sensitivity using several percentiles at 0, 1, 5, 25, 50, 75, 95, 99 and 100%; these are selected using one scenario so that scenarios can be compared against each other. In this framework we also output CO_2 concentrations from FaIR for use in JULES, in future work we intend to explore the selection of ensemble members based on sampling the CO_2 range of uncertainty as well as temperature but this is not explored here. In this paper, we present just one way that the user can choose to run PRIME but these choices are not intrinsic to PRIME as a framework. The optimal sampling strategy within the distribution of FaIR outputs and climate patterns (see 2.2) can and will vary on a case-by-case basis depending on the desired use of the framework. Additionally all the percentiles are available from FaIR if a user chooses to use them.

2.2 Spatial patterns and temporal downscaling of climate change

In PRIME, we use an early version of pattern-scaling developed by Huntingford and Cox (2000). We derive relationships for eight variables (near-surface air temperature, diurnal temperature range, precipitation, shortwave radiation, longwave radiation, near-surface specific humidity, 10m wind speed, and surface pressure) by linear regression at each grid cell, using global mean temperature change as the predictor and anomalies relative to the 1850–1889 mean. Monthly patterns for each of 34 CMIP6 models (see Supplementary Table S1) are calculated, using the SSP5-8.5 emissions scenario: sampling the CMIP6 ensemble's range of uncertainty. We generate the patterns separately for each CMIP model (using the recipe available in ESMValTool see the data availability section), the regression is calculated with points from the duration of SSP5-8.5, from 2015-2100. We then use the IMOGEN code within JULES to generate the 3-hourly data with which to run the JULES land surface model. This means that PRIME is run for each CMIP pattern individually (we do not run it using the average CMIP pattern). This use of a large proportion of the CMIP6 ensemble means that PRIME considers all combinations of GCM output for a broad range of climates represented by the CMIP6 ensemble. Wells et al. (2023) show that whilst selecting patterns derived from emissions scenarios with radiative forcings closer to the target scenario results in the lowest emulation errors, the best all-round performance is obtained by using a high warming scenario to obtain the patterns, hence our choice of SSP5-8.5 as our training scenario. For further detail on the patterns evaluation, see Section 3.2. We include all input variables, even those that do not typically pattern scale as well because these are known to have less influence in JULES and this is the method currently used in PRIME to produce sub-daily data to run the JULES land-surface model (see Section 3.2).

The spatial distribution of the meteorological driving data for JULES is reconstructed from the climate patterns multiplied by the global mean temperature change (Section 2.1) superimposed on an observed monthly climatology. The observed monthly climatology was constructed from the daily meteorological data provided by the GSWP3-W5E5 dataset from the ISIMIP3a project (Frieler et al., 2023) for the period 1901–1930. This was regridded to a resolution of N48 with a 3.75° longitude grid size and a 2.5° latitude grid size. We then use the weather generator that is built into IMOGEN to downscale to the hourly timescale and accurately simulate the diurnal cycle and exchange of heat, water and momentum and to avoid numerical

instabilities (Williams and Clark, 2014); this is similar to the disaggregator described in Mathison et al. (2022). The diurnal cycle in near surface air temperature is defined using:

$$T = T_o + \frac{\Delta T}{2} cos\Big(\frac{2\pi(t - t_{T_{max}})}{T_{day}}\Big) \quad (1)$$

where T_o and ΔT are the temperature and diurnal temperature ranges respectively. T_{day} is the length of the day, $t_{T_{max}}$ is the time of day when the temperature is highest. $t_{T_{max}}$ is calculated from the following equation which assumes that it occurs 0.15 of a day length after solar noon:

$$t_{T_{max}} = \frac{t_{up} + t_{down}}{2} + 0.15(t_{up} - t_{down}) \quad (2)$$

where t_{up} and t_{down} are sunrise and sunset times. The downward shortwave radiation which includes the diurnal cycle is the daily mean downward shortwave radiation multiplied by a solar radiation normalisation factor which depends on the position of the sun in the sky at each timestep for each gridbox. This means that sub-daily downward shortwave radiation and temperature are estimated using these known factors and a sinusoidal function to represent the maximum and minimum daily range.

The downward longwave radiation which includes the diurnal cycle (R_{lw}) is a linear function of temperature (Huntingford et al., 2010) and is derived assuming black body radiation and that the diurnal cycle of temperature is negligible:

$$R_{lw} = R_{lw,o} + \Big(\frac{4T}{T_o} - 3\Big) \quad (3)$$

where $R_{lw,o}$ is the downward longwave radiation before temporal disaggregation.

The IMOGEN weather generator distributes monthly mean rainfall subject to a probability distribution that has fixed parameters in time (i.e. year), although dependent on month and location. For each year, a random number generator is applied to sample from the distribution. The distribution parameters are fitted to known historical gridded measurements of precipitation. Precipitation is split into 3 types: large-scale rain, convective rain and large-scale snow and considered to occur in a single event, with a globally specified duration parameter (6 h for convective rainfall, 1 h for large-scale rainfall and convective snowfall and large-scale snowfall). The type of precipitation at any particular time depends on the mean daily temperature. If the daily temperature is greater than 293.15 K it is convective rain, between 275.15 K and 293.15 K it is large scale-rain and below 275.15 K it is large scale-snow. This precipitation is divided into events of randomly generated duration. If the maximum precipitation rate in any timestep is greater than 350.0 mm/day, the precipitation is again redistributed to reduce these values to less than the threshold.

2.3 Land Surface and Impacts Model

The Joint UK Land Environment Simulator Earth System (JULES; Best et al., 2011; Clark et al., 2011; Wiltshire et al., 2021) land surface model is a community model used both in standalone model and as the land surface component of the UK Earth System Model (UKESM; Sellar et al., 2019). Here, JULES is used in standalone mode, driven by climate data reconstructed by

combining the monthly patterns derived from the ESMs and the global mean temperature change from FaIR. The configuration of JULES used here is denoted JULES-ES (Mathison et al., 2022) and is the configuration used in both UKESM1 (Sellar et al., 2019) and to provide simulations for the Inter-Sectoral Impact Model Intercomparison Project (ISIMIP) in Mathison et al. (2022). In PRIME JULES-ES is also driven by the CO_2 concentration output from FaIR.

JULES-ES has 9 natural plant functional types (PFTs; 5 types of trees, C3 and C4 grasses, and evergreen and deciduous shrubs) and four managed PFTs (C3 and C4 crop and pasture), where the managed PFTs are set to their observed values at 2005. The Top-down Representation of Interactive Foliage and Flora Including Dynamics (TRIFFID) dynamic vegetation model (Cox, 2001) determines the proportion of each PFT present in a grid cell. Nitrogen limitation on ecosystem carbon assimilation is represented in JULES-ES (Wiltshire et al., 2021). External nitrogen inputs are via biological nitrogen fixation and nitrogen deposition, and losses are via leaching and a gas loss term. Nitrogen limitation reduces the carbon-use efficiency of the vegetation via a reduced net primary productivity and can slow soil decomposition. The soil biogeochemistry is represented by a single bulk layer with four soil pools: two litter pools, a microbial biomass pool, and a humus pool each with an equivalent organic nitrogen pool. Inorganic nitrogen is converted from organic nitrogen and can be taken up by the plants.

3 PRIME evaluation

In this section, we evaluate PRIME. In this context, that means that we want to use PRIME to produce land simulations for scenarios where ESMs have not been run, but we can test it in cases where ESM simulations do exist. Here, we use CMIP6 simulated output for a range of different but well known future climate scenarios: SSP1-2.6, SSP5-3.4-OS (these are verification scenarios) and SSP5-8.5 (this is the training scenario). We show that PRIME gives close agreement of global temperature and spatial patterns of climate giving us confidence in its ability to be used to project as-yet un-simulated scenarios. We also compare simulated land-surface output from PRIME with that from CMIP6 for ESMs that have reported the required diagnostics.

PRIME has 3 distinct and independent steps, as described in Section 2: (i) timeseries of global temperature are produced from FaIR based on emissions of greenhouse gases and aerosols, (ii) spatial patterns of climate change are constructed from the global temperature based on CMIP simulations, and (iii) these climate patterns are used to drive JULES to simulate land surface outcomes. In this section, we present evaluation of these three steps and at each step assess the agreement with existing output from CMIP6 or the IPCC AR6 assessment using various standard statistical methods. The chosen statistics vary with each step and includes the mean absolute error (MAE), the root mean square error (RMSE), the Pearson correlation coefficient, and the interquartile range (IQR) of model predictions.

3.1 Emulation of global temperature change

For the first time, IPCC AR6 was able to apply multiple lines of evidence to constrain future projections of global temperature from the CMIP6 ensemble. As such, the spread of global temperature in 2100 is smaller than if taken from raw CMIP6 ESM output (Lee et al., 2021). We compare the simulated global temperature from PRIME (run with emissions) with the constrained

range assessed by IPCC (see Figure 4.11 and Table 4.5 of Lee et al. (2021)) in Figure 2. The FaIR simulations used here do not include solar and volcanic fluctuations, instead focusing on the anthropogenic forcing, which is the main driver of human-induced effective radiative forcing and human-induced warming (Forster et al., 2023). The left panel shows the mean Global mean Surface Air Temperature (GSAT) from FaIR (solid lines) and 5th and 95th percentiles (shaded region). The right panel shows the mean and 5–95th percentile for the period 2090–2100 relative to 1850–1900 for each SSP scenario (we include the same scenarios here to enable comparison with the same plot in the IPCC report): SSP1-1.9, SSP1-2.6, SSP2-4.5, SSP3-7.0 and SSP5-8.5 for FaIR end of century GSAT values and the IPCC constrained values. The end of century ranges in PRIME are close to the IPCC ranges with the timeseries and model spread consistent with the IPCC constrained range.

The uncertainty in projected global mean temperature arises from uncertainty in both physical and biogeochemical feedbacks like the carbon cycle. We know atmospheric CO_2 is an additional direct driver of impacts, therefore this is another output from FaIR that is included in PRIME as an input to JULES-ES. PRIME samples the joint distribution of CO_2 and global temperature from the constrained FaIR ensemble. Figure 3 shows how the ensemble members selected span the distribution for SSP1-2.6 (similarly the joint distribution of CO_2 and temperature are also shown in the Supplementary information Fig. S1 for SSP5-3.4-OS; left and SSP5-8.5, the training scenario; right). As our primary aim is to sample future impacts associated with uncertain future temperature outcomes, we sub-sample the 2100 FaIR temperature distribution for the impacts modelling. This results in a co-sampling of CO_2 levels that does not span the full uncertainty in resulting CO_2 concentrations. This is not a limitation of PRIME - other applications could use a different sampling strategy or use the full ensemble of 2237 members. As mentioned in Section 2.1, the sampling strategy will depend on the intended application of the framework, the use of both temperature and CO_2 concentration from the FaIR distribution is discussed in Section 5.

3.2 Spatial patterns of climate change

Emulated climate patterns are evaluated against their CMIP6 equivalents for a number of scenarios. Alongside global comparison, four example regions are chosen to test the pattern evaluation at regional scales: the Amazon basin, the Siberian forest, India and the United States of America. These regions span tropical and boreal ecosystems, temperate regions and a region dominated by a Monsoon climate. The climate patterns were evaluated against the out-of-sample CMIP6 runs of the SSP1-2.6 and SSP5-3.4-OS scenarios as SSP5-8.5 was used to train the pattern scaling.

Climatologies of each CMIP6 model were calculated by taking the mean of the period 1850–1889 inclusive. Anomalies were then calculated by subtracting the climatologies from the spatiotemporal CMIP6 datasets, ensuring that the variants of the historical runs matched those of the scenarios. To compare against these, predicted patterns for each ESM were compiled by multiplying annual mean GSAT data by pattern values at each grid point (see Methods, Section 2.2), creating a spatiotemporal dataset of anomalies for each variable (see Table 1). The predicted patterns were then evaluated against the anomaly datasets from CMIP6. The number of models included in the evaluation depends on the scenario, as not all CMIP6 models simulated every SSP. Here, 29 models are included in the evaluation against SSP1-2.6 and 15 are included in the evaluation of SSP5-3.4-OS, out of the 34 available model patterns.

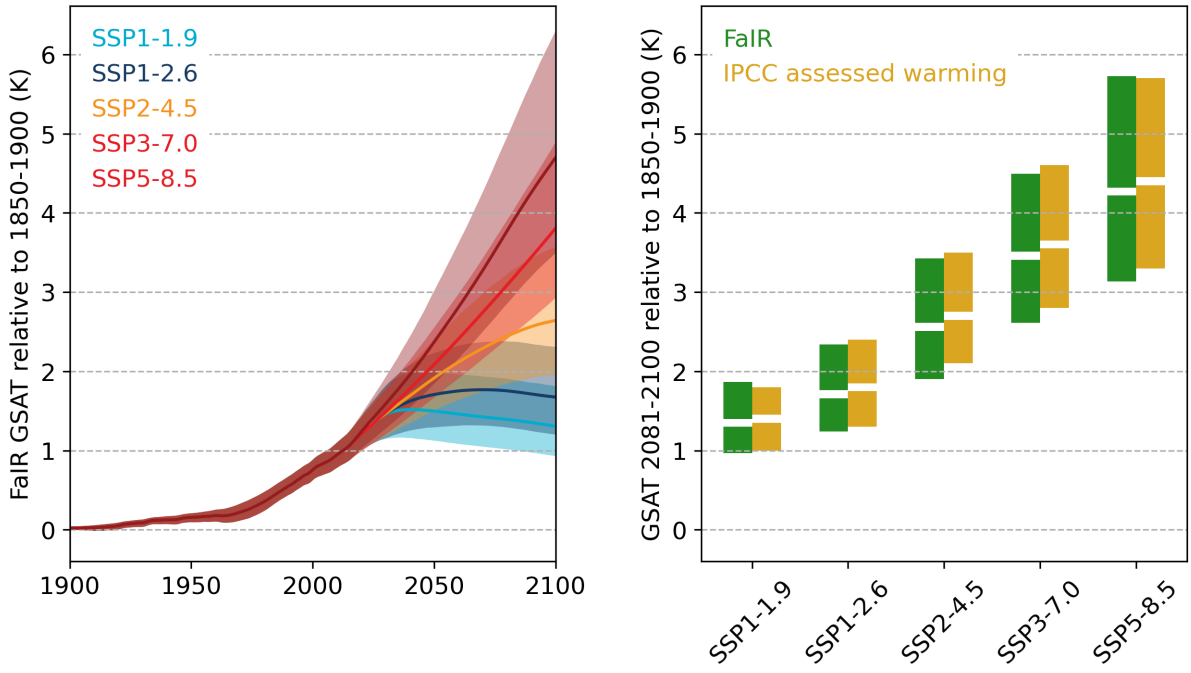

Figure 2. (a) Projected global temperature from FaIR for five SSP emissions scenarios, and (b) comparison of end-of-century (2080–2100) mean warming from FaIR (green) and IPCC AR6 assessment (yellow; Figure 4.11 and Table 4.5 of Lee et al. (2021))

.

Our evaluation of the emulated patterns focuses on the ability to capture the mean and spread of the CMIP6 ensemble. The aim is for PRIME to appropriately capture the response to forcing across a range of scenarios and also the spatial uncertainty. We evaluate the pattern scaling by comparing mid (2040-2060 mean) and end of century (2080-2100 mean) predictions for all variables against CMIP6 anomalies for two out-of-sample scenarios: SSP1-2.6 and SSP5-3.4-OS using pattern predicted ensemble means compared to the CMIP6 ensemble mean anomalies. In Figure 4 we show evaluation of predictions of near-surface air temperature and precipitation. The right hand column shows the error in our prediction of the CMIP6 multi-model mean. Temperature is clearly seen to scale well, with small errors during both the mid and end of centuries, however warming in the northern latitudes is generally slightly underestimated across both timescales. The results for precipitation show much more spatial variance. Patterns of change are well-captured during both timescales, as can be seen in Fig. 4 (d, e, and j, k), though prediction errors do occur for some regions (see Fig. 4 f, l), for example in the Amazon, where rainfall is generally underestimated, Southern Africa where it is overestimated and South-east Asia, where differences vary over timescales. We include further evaluation of patterns for the other JULES input variables in the supplementary information (see Figures S2 for specific humidity and wind, S3 for pressure and downwelling shortwave radiation and S4 for downwelling longwave radiation and the diurnal temperature range). We also show all variables for SSP5-3.4-OS in the Supplementary Information (these are shown in the same order with temperature and precipitation first in Figures S5 to S8). We also show the training scenario,

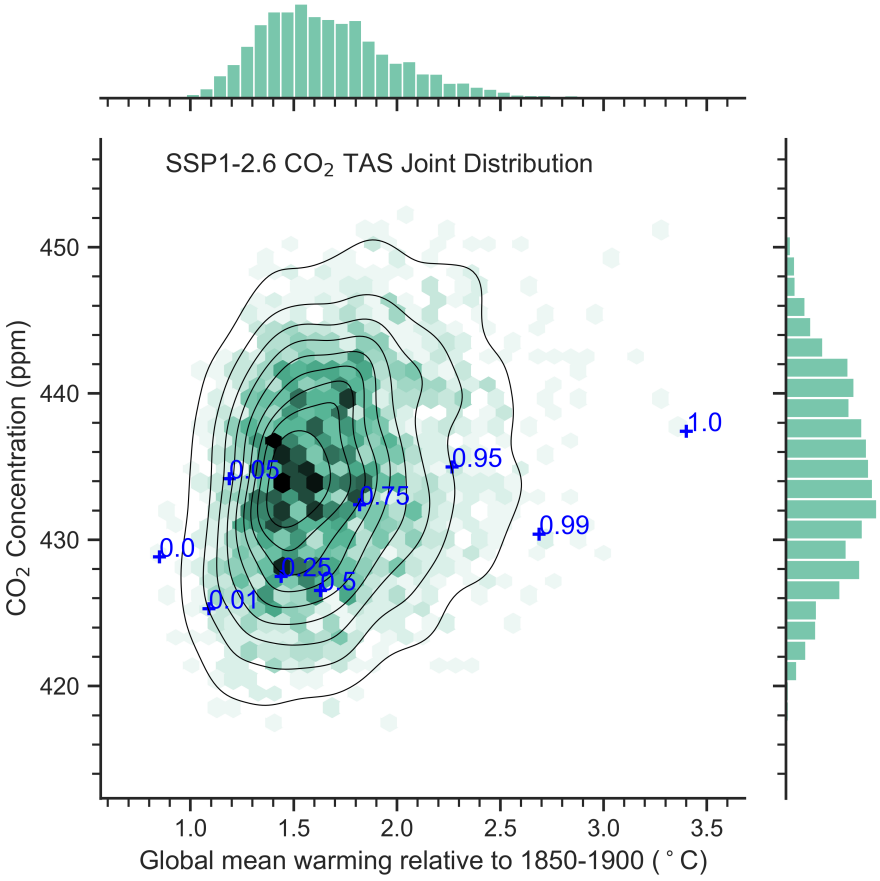

Figure 3. Joint frequency distribution of global temperature rise and CO_2 concentration in 2100 for SSP1-2.6 emissions and the sub-selected percentiles (blue crosses) used to drive the JULES impacts model. Shades of green denote the density of points with individual histograms above and to the right of the main panel. 10% confidence intervals are shown by the contours.

SSP5-8.5, in the supplementary information for temperature and precipitation (see Figure S9) as a sanity check. In general, errors in pressure (Figure S3, a-c and g-i), longwave downwelling radiation (Figure S4, a-c and g-i) and specific humidity (Figure S2, a-c and g-i) tend to be smaller while errors in shortwave downwelling radiation (Figure S3, d-f and j-l), wind (Figure S2, d-f, j-l) and the diurnal temperature range (Figure S4, d-f and j-l) tend to be larger, regardless of the scenario and particularly at the end of the century (k and l). For downwelling shortwave radiation particularly, this is likely to be due to the influence of other factors such as aerosols.

In addition to evaluating the relative ensemble means, it is important to check that prediction errors fall within the range of responses seen in CMIP6. We therefore check that the absolute error in our predictions is small compared to the spread in the ensemble predictions. We calculate the absolute error of each model's prediction against its CMIP6 counterpart and take the

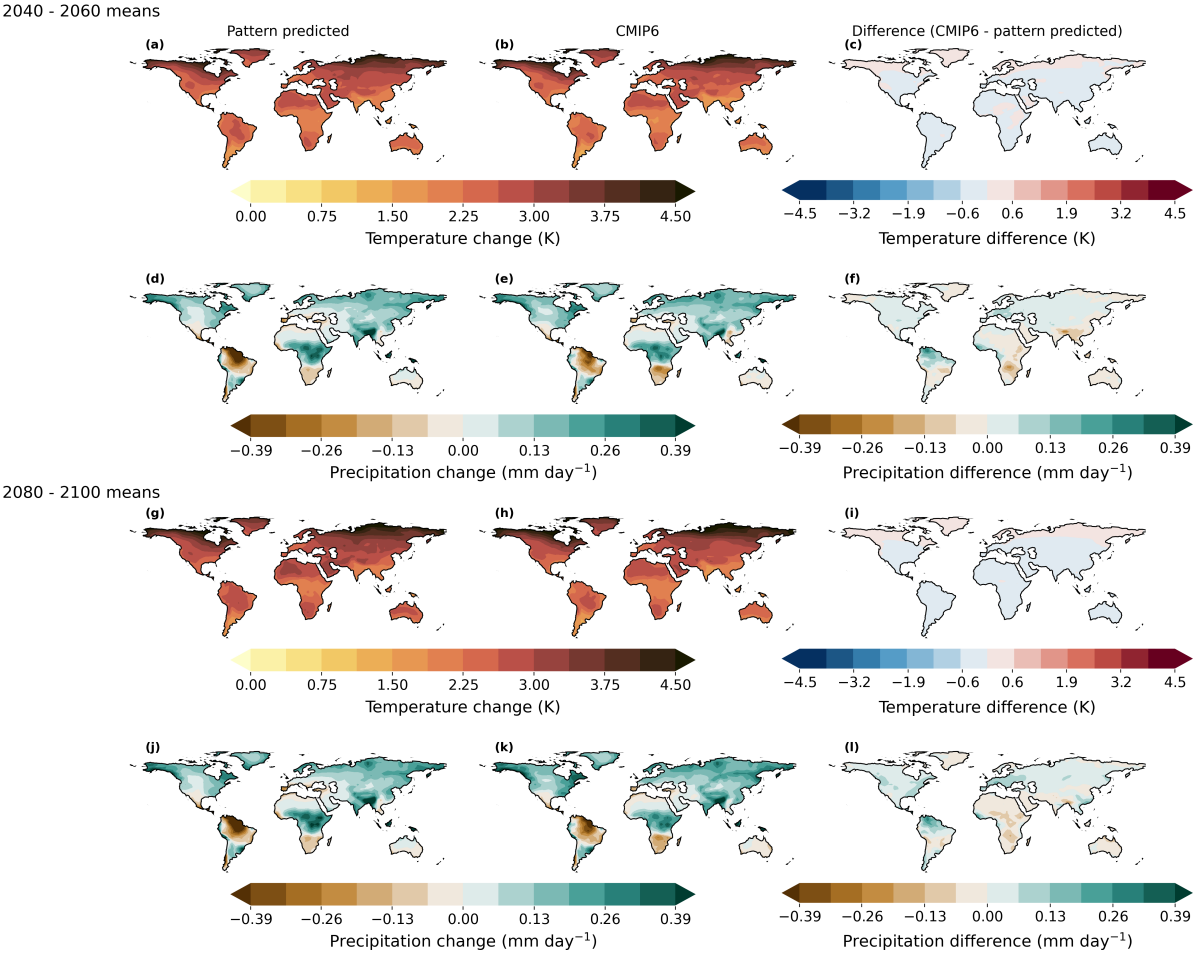

Figure 4. Evaluation of the pattern predicted ensemble means compared to the CMIP6 ensemble mean anomalies for near-surface air temperature **(a-c, g-i)** and precipitation **(d-f, j-l)** for SSP1-2.6. Maps **(a-f)** highlight mid-century predictions, and **(g-l)** show those for the end of century. The right hand column shows the difference between the predictions (left hand column) and CMIP6 (middle column). The colourbar magnitude for the differences is the same as that for the anomalies, in order to show that the prediction error is small compared to the change induced by the scenario.

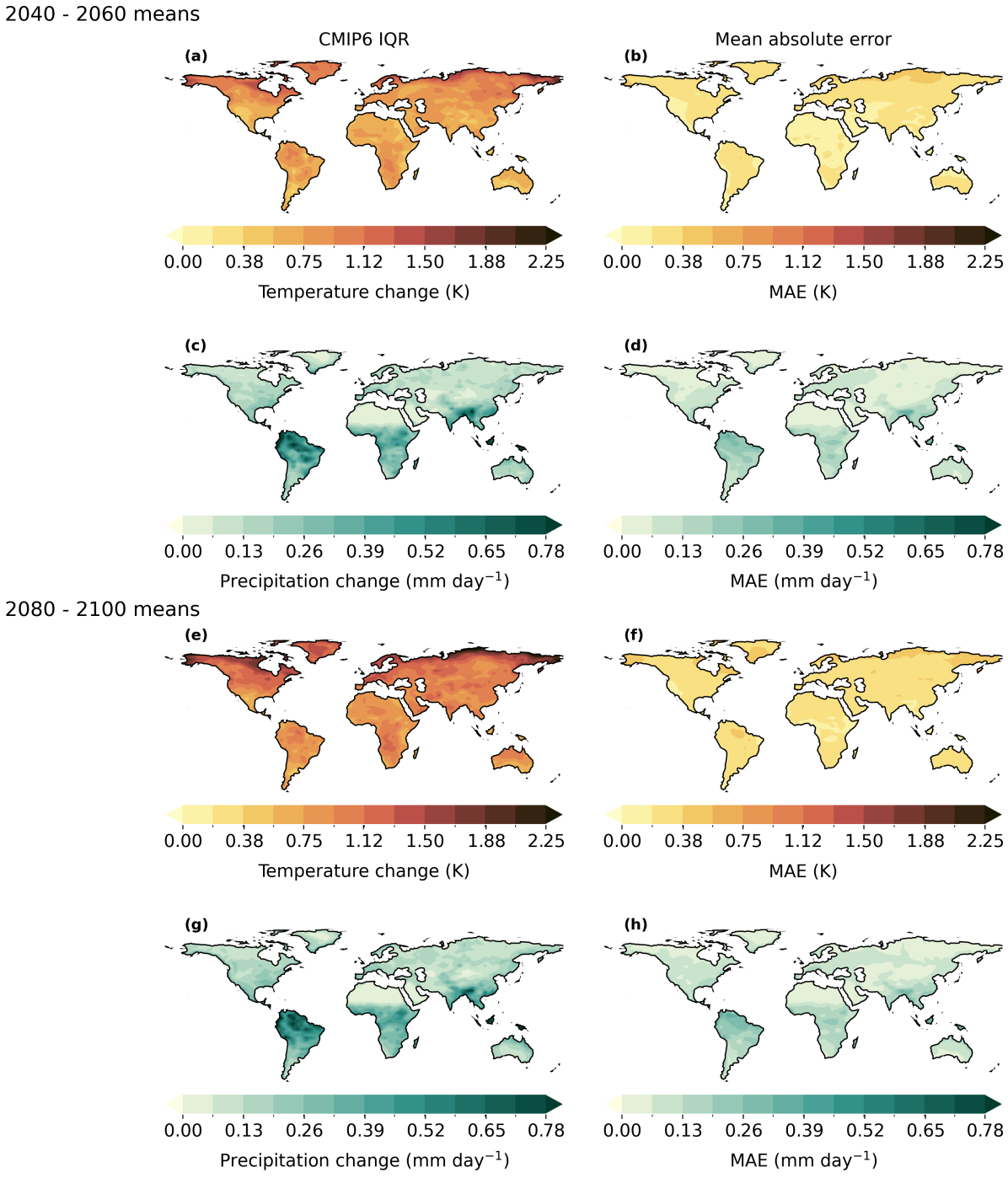

Figure 5. Evaluation of the interquartile range (IQR) of predictions and of the mean absolute model-to-model error (MAE) for SSP1-2.6 for temperature **(a,b,e,f)** and precipitation **(c,d,g,h)**. Maps **(a-d)** highlight mid-century predictions, and **(e-h)** show those for the end of century. The right hand column shows the MAE.

Table 1. Summary table for evaluation section: Root Mean Square Error (labelled RMSE) between multi-model mean pattern predictions and CMIP6 both at mid century (labelled Mid i.e 2040-2060) and end of century (labelled End i.e. 2080-2100) for values on land across the globe for each input variable and scenario. RMSE is spatially aggregated across months and models.

Variable	Units	SSP1-2.6		SSP5-3.4-OS		SSP5-8.5	
JULES inputs		RMSE		RMSE		RMSE	
		Mid	End	Mid	End	Mid	End
Temperature	$^{\circ}C$	0.43	0.52	0.42	0.53	0.34	0.35
Specific Humidity	g kg^{-1}	0.0001	0.0002	0.0001	0.0002	0.0001	0.0001
Precipitation	mm day^{-1}	0.20	0.22	0.22	0.22	0.18	0.17
Wind	m s^{-1}	0.10	0.11	0.10	0.11	0.09	0.08
Pressure	kg m^{-1} s^{-2}	32.11	36.79	36.29	34.53	28.55	25.81
Shortwave radiation	W m^{-2}	1.75	2.16	1.85	2.19	1.88	1.98
Longwave radiation	W m^{-2}	1.88	2.29	1.74	2.25	1.52	1.65
Diurnal temperature range	$^{\circ}C$	0.12	0.13	0.09	0.11	0.09	0.09

mean over the ensemble at each gridpoint. If the mean absolute error (MAE) is low relative to the CMIP6 IQR, it suggests the pattern scaling technique is not adding significant variation in its predictions beyond that driven by the differences between the patterns. We can therefore be confident that despite deficiencies, the ensemble approach is adding useful information on the uncertainty and spread. Figure 5 shows that the MAE is smaller than the ensemble range for temperature and precipitation in the mid and end of century for SSP1-2.6. The range in error of precipitation predictions is higher and more heterogeneous than temperature, although the spatial patterns are similar across timescales. The tropics in particular are regions of higher MAE, which is reflective of the differences in the underlying model patterns for these areas, although the MAE is still seen to be smaller than that of CMIP6. Table 1 shows the mid and end of century RMSE values for each input variable for JULES. RMSE is a standard measure of the error in the predicted variable relative to the mean change. From previous analysis of the JULES input variables, it is known that there are some variables that are more important for JULES. For example, temperature, specific humidity and precipitation are key drivers with other input variables like wind speed, pressure and longwave downwelling radiation having less influence. This means that even though the pattern scaling for some of these variables may have greater error, they are not as important because JULES is known to be less sensitive to these. Overall, the pattern scaling captures the pattern of change well for the key JULES variables, with the training scenario, SSP5-8.5 having the greatest agreement. This is as expected because this was used to generate the patterns but also this is the scenario with the strongest climate change signal. The relative error increases in the lower scenarios related to the need to predict a smaller signal (Wells et al., 2023; Kravitz et al., 2017). However, the low RMSEs for these key variables give us confidence to apply the pattern scaling to different scenarios including stabilisation and overshoot pathways. In future work, we would also like to explore the impact of including

the patterns for all of the JULES input variables on the outputs from PRIME in a sensitivity analysis, to understand if the input variables that do not pattern scale well but are less important for running JULES affect the spread of the results from PRIME.

In addition, we evaluate if PRIME pattern scaling can also reproduce the range of changes across the CMIP6 ensemble for all JULES input variables. In several figures we compare timeseries and end of century predicted changes across CMIP6 ESMs for all variables and four regions. Temperature and precipitation are shown in Fig. 6 and 7 with other six variables in Figures S18 to S23 in supplementary information. The multi-model mean pattern, per °C of warming, is shown in the central map for temperature (Fig. 6) and precipitation (Fig. 7). Burton et al. (2020) show that temperature and precipitation are two of the primary drivers of the response of land-surface processes to climate change. For each region and variable, the figures show timeseries of change for that region as a shaded plume of CMIP6 output (blue) and predicted by pattern-scaling (pink). The end-of-century values for each CMIP6 model individually are shown as a scatter-plot for each variable, region and scenario to illustrate the agreement between pattern-scaled and actual values (see Fig. 6 for temperature and precipitation inFig. 7). The end of century Pearson correlation values illustrated by the scatter plots in Figures 6 and 7 are also given, along with the RMSE in the regional tables, Table 2 and 3 for temperature and precipitation. The Pearson correlation coefficient is a widely used measure of the strength of the linear relationship between two variables, we use it here to quantify the linearity of the pattern predictions against CMIP6 for each model with respect to the one-to-one line. For temperature (Fig. 6) the range of future projections across CMIP6 models spans approximately 5-10 °C warming by 2100 under SSP5-8.5 for each region, with high-latitudes warming more than the tropics as expected. The PRIME pattern-scaled ensemble does well to reproduce this range of projections across the CMIP6 ensemble, with points lying close to the 1-to-1 line for all regions and scenarios. Pearson correlation coefficients for between-model predictions exceed 0.93 for all regions and scenarios (Table 2), with SSP5-8.5 fitted the best. This is expected as the patterns were derived from this scenario. Importantly, this gives confidence that the PRIME system is not introducing any significant errors particularly in the training scenario and that the pattern scaling accurately reproduces the spread of results, model-by-model of the CMIP6 ensemble for this scenario.

Results for precipitation (Fig. 7) also show good agreement, but some mismatches appear as precipitation is more variable in space and time than temperature, as seen in the higher error characteristics in the pattern scaling and slightly lower correlation coeefficients in Table 3. Nevertheless, PRIME predicts well the signal of increasing precipitation over the United States, Siberia and India and reduced rainfall over the Amazon Basin. Again, the range and spread of results across the CMIP6 ensemble are well matched, and the correlation coefficients shown in Table 3 are reasonable and above 0.75 for all regions and scenarios.

Across-model spread of the other variables (Figures S18 to S23 of the Supplementary information) is also well captured by PRIME pattern scaling. Changes in humidity (Fig. S18) are well reproduced, while wind speed changes (Fig. S19) has mixed skill being poorly captured over United States, despite changes in surface pressure (Fig. S20) being well reproduced for all regions. The most notable departure of predicted and actual changes occurs for surface downwelling shortwave radiation (i.e. incoming solar radiation shown in Fig. S21). For all regions and scenarios, the end-of-century values match well, but the significant dip in shortwave radiation during the historical period is not seen at all in the predicted patterns. This period of "global dimming" (Wang et al., 2022; Stanhill and Cohen, 2001) is well known to be caused by anthropogenic aerosols and cannot be replicated by scaling global temperature. Features such as this are an obvious limitation of a pattern scaling approach

Table 2. Root Mean Square Error (RMSE in °C) and Pearson correlation coefficient (Pearson) between pattern predicted and CMIP6 end of century temperature change (see Figure 6 for scatter plot for each region showing each model) for each scenario. Average values over region of interest compared to its CMIP6 equivalent by model.

Region	SSP1-2.6		SSP5-3.4-OS		SSP5-8.5	
	RMSE	Pearson	RMSE	Pearson	RMSE	Pearson
Amazon	0.27	0.96	0.22	0.98	0.13	0.99
Siberia	0.33	0.93	0.28	0.98	0.23	0.99
USA	0.21	0.95	0.21	0.98	0.21	0.99
India	0.29	0.93	0.21	0.97	0.37	0.98

Table 3. Root Mean Square Error (RMSE in mm day^{-1}) and Pearson correlation coefficent (Pearson) between pattern predicted and CMIP6 end of century precipitation change (see Figure 7 for scatter plot for each region showing each model) for each scenario. Average values over region of interest compared to its CMIP6 equivalent by model.

Region	SSP1-2.6		SSP5-3.4-OS		SSP5-8.5	
	RMSE	Pearson	RMSE	Pearson	RMSE	Pearson
Amazon	0.12	0.77	0.11	0.85	0.079	0.98
Siberia	0.045	0.86	0.036	0.96	0.022	0.99
USA	0.065	0.75	0.056	0.83	0.037	0.96
India	0.094	0.87	0.081	0.93	0.13	0.94

which does not account for different regional patterns from different climate forcers such as aerosols. Finally, changes in downwelling long-wave radiation (Fig. S22) and diurnal temperature range (Fig. S23) are well captured across regions and scenarios by the PRIME pattern scaling.

In conclusion, the patterns both for each CMIP6 ESM and the range of changes across ESMs are generally well reproduced by the PRIME pattern scaling technique. This is true for each of the four distinct regions and three very different emissions scenarios. The pattern scaling technique is simple and well understood by the literature, and here we find it largely capable of spatially downscaling the global climate response in out-of-sample low-signal and overshoot scenarios.

3.3 Land Surface and Impacts Simulation

The final section of the PRIME evaluation shows the results using the FaIR produced projections of global mean surface temperature together with the scaled climate patterns, to drive the JULES land surface model. The JULES step of PRIME is evaluated using two climate variables as examples of output produced by most ESMs. End of century changes projected by PRIME are compared against the equivalent ensemble mean CMIP6 data. The example variables considered help us to assess the carbon and hydrological cycles: Gross Primary Productivity (GPP), which is the gross rate of accumulation of carbon via photosynthesis, and runoff (mrro), which is the excess water not absorbed by soils and accumulated by water sources.

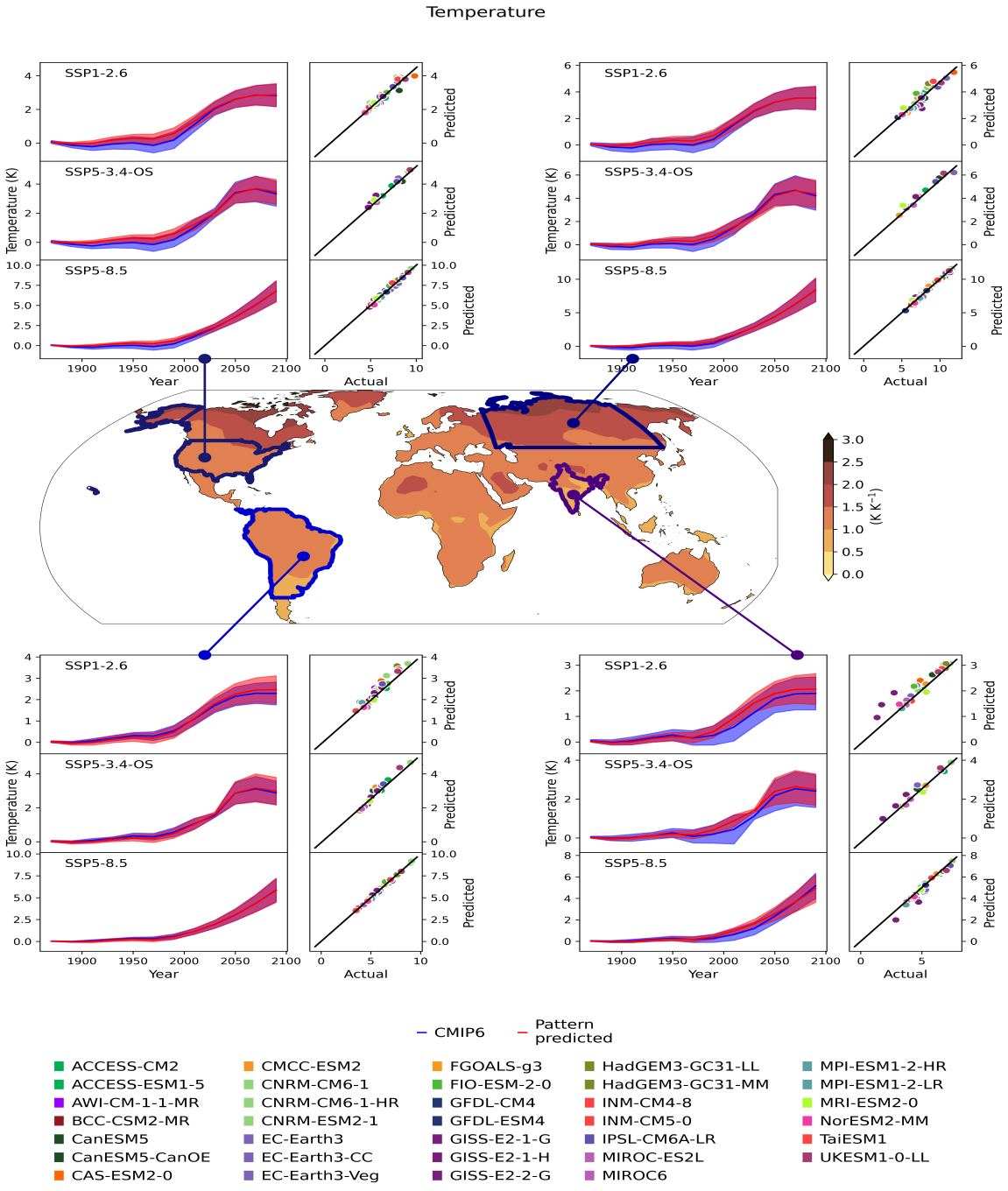

Figure 6. The central map shows the temperature pattern (where there is no hatching indicates that the models tend to agree on the sign of the change and with hatching to show where the models tend to disagree on the sign of the change), and subpanels for each region: North America, Siberia, South America and South Asia. The region subpanels show the temperature timeseries (left subpanel) and scatter plots (right subpanel) for each scenario; top: SSP1-2.6, middle: SSP5-3.4-OS and bottom: SSP5-8.5 (the training scenario). The timeseries shows the PRIME patterns (blue plume) and the CMIP6 patterns (red plume). The scatter plots show the end of century values predicted by PRIME vs CMIP6 actual values for each model with the model colours shown at the bottom of the figure.

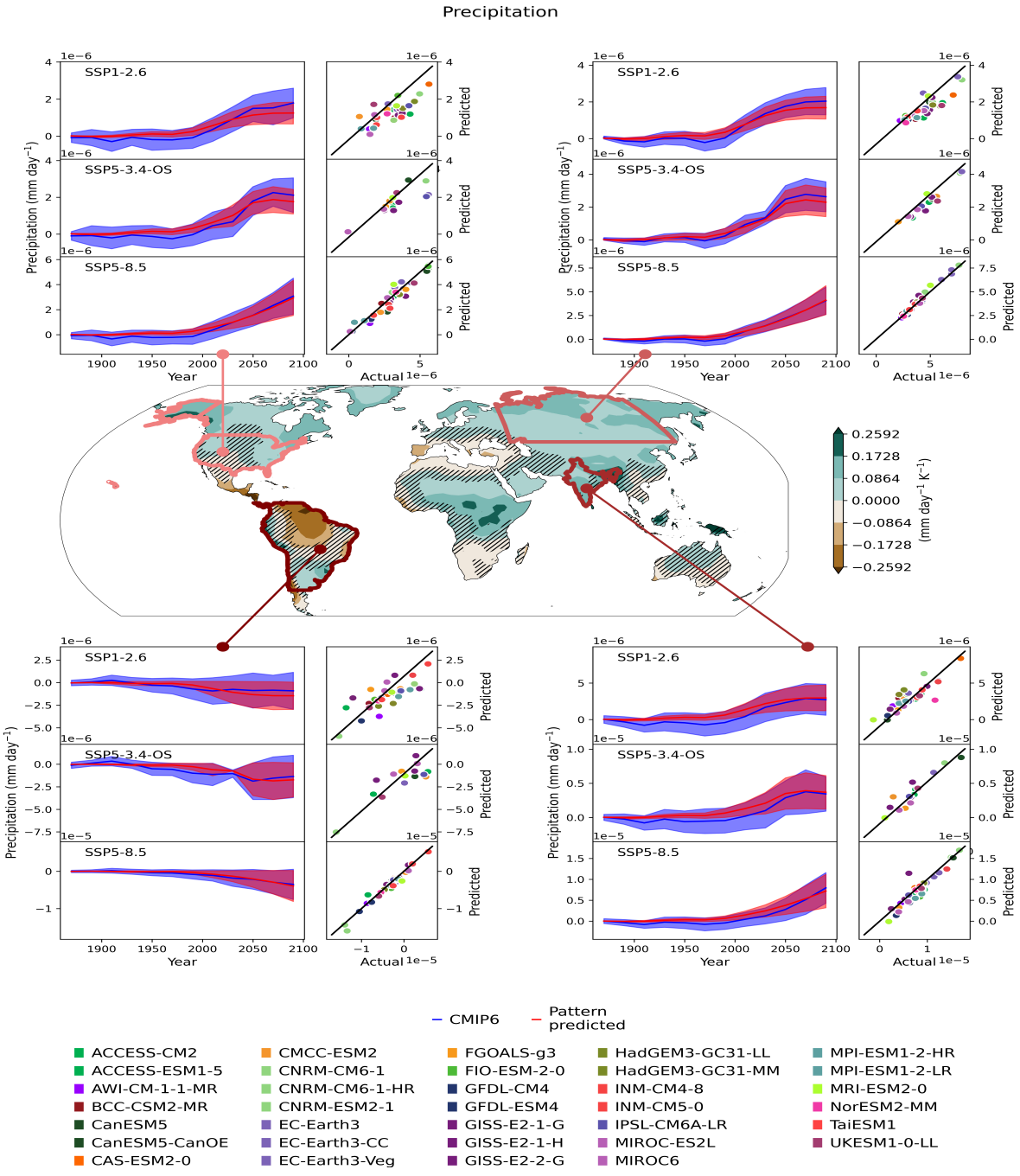

Figure 7. The central map shows the precipitation pattern (where there is no hatching indicates that the models tend to agree on the sign of the change and with hatching to show where the models tend to disagree on the sign of the change) and subpanels for each region: North America, Siberia, South America and South Asia. The region subpanels show the precipitation timeseries (left subpanel) and scatter plots (right subpanel) for each scenario; top: SSP1-2.6, middle: SSP5-3.4-OS and bottom: SSP5-8.5 (the training scenario). The timeseries shows the PRIME patterns (blue plume) and the CMIP6 patterns (red plume). The scatter plots show the end of century values predicted by PRIME vs CMIP6 actual values for each model with the model colours shown at the bottom of the figure.

For this stage of evaluation, we do not expect as good a match with CMIP6 outputs as obtained for the driving climate variables in Section 3.2. This is because PRIME uses the JULES land-surface model which will differ from the embedded land schemes in the different CMIP6 ESMs. We perform this comparison for two example variables to demonstrate the extent to which the PRIME framework can reproduce the range of simulated land behaviour from CMIP6, but can not expect a perfect match. Future work to include other land models or perturbed parameter ensembles of JULES would help address potential mismatches.

Figure 8 shows the multi-model mean projected end of century changes in GPP and runoff in the SSP1-2.6 scenario, the first of two verification scenarios, using both the PRIME framework and CMIP6. Figures S24 and S25 in the Supplementary information show the equivalent results for scenarios SSP5-3.4-OS (a second verification scenario) and SSP5-8.5 (the training scenario) respectively. The similarity in the predicted spatial patterns can be seen, where in the majority of regions, PRIME matches the pattern of change projected by CMIP6. As we did for climate patterns, we evaluate within and across CMIP6 ESMs. Table 4 presents the mean and interquartile range for both the PRIME and CMIP6 ensemble for each output variable considered. We would not expect these values to be identical but we hope for a similar spread and mean for both GPP and runoff, which we do see in the values in Table 4. Some deviations are seen between the projections; for example, PRIME projects greater magnitudes of change in both runoff and GPP in the tropical regions compared to CMIP6 (Fig. 8). To put these changes into context from a carbon perspective, PRIME exhibits an end of century global increase in GPP in SSP1-2.6 of 26 (between 18 and 34) GtC yr^{-1}, while CMIP6 increases by 30 (between 15 and 43) GtC yr^{-1}, compared to pre-industrial. For the training scenario, SSP5-8.5, for PRIME the end of century increase is 77 (between 58 and 98) GtC yr^{-1}, while CMIP6 increases by 70 (between 37 and 99) GtC yr^{-1}, compared to pre-industrial. Therefore in both the out of sample scenario and the training scenario PRIME broadly captures the range shown by the CMIP6 ensemble.

Table 4. Summary table for JULES outputs: mean and Inter-quartile range (IQR) for CMIP6 and PRIME for end of century values on land across the globe.

Variable	Units	SSP1-2.6		SSP5-3.4-OS		SSP5-8.5	
JULES outputs		CMIP	PRIME	CMIP	PRIME	CMIP	PRIME
		Mean	Mean	Mean	Mean	Mean	Mean
		(IQR)	(IQR)	(IQR)	(IQR)	(IQR)	(IQR)
Gross primary	kg m^{-2} yr^{-1}	0.22	0.18	0.27	0.24	0.52	0.54
productivity		(0.32)	(0.33)	(0.43)	(0.41)	(0.71)	(0.87)
Runoff	m^3 day^{-1} x10^{-4}	0.59	0.55	0.82	0.78	1.61	2.17
		(1.22)	(1.00)	(1.52)	(1.32)	(2.73)	(2.94)

Across CMIP6 models, projections are compared in the four specific regions (Amazon, Siberia, USA and India) for both variables (Supplementary Figures S26-S29 for SSP1-2.6 and S30-S33 for the training scenario, SSP5-8.5). PRIME-simulated GPP and runoff can be compared on a model-by-model basis. The results shown in figures in the Supplementary information (Figures S26-S33) for each region show CMIP6 output for each ESM and the corresponding PRIME simulated output from

JULES using the climate patterns from the same ESM. For GPP (top row in Supplementary information Figures S26-S33), the PRIME-simulated changes are typically simulated well, although JULES has a tendency to simulate greater increases in GPP than many of the CMIP6 models. A couple of CMIP6 ESMs clearly stand-out. The blue/green coloured lines showing the CNRM and MPI variants in CMIP6 consistently simulate greater increases in GPP than JULES. This does not signal an error in PRIME, just that the different land models simulate different sensitivity to future climate changes. PRIME does though, mainly reproduce the signal and spread of GPP for all regions and scenarios simulated by CMIP6.

Runoff for three of the four regions is well reproduced in PRIME (bottom row in Supplementary information Figures S26-S33), where: Siberia (Figure S27 and S31), United States (Figure S29 and S33) and India (Figure S28 and S32) all see steady increases in runoff consistent with increases in precipitation in those regions. JULES output agrees with these changes of simulated magnitude and spread. The Amazon basin region (Figure S26 and S30) though exhibits some notable differences. Figure 7 (bottom left) shows a range of precipitation responses over the Amazon with an overall consensus of a drying signal (see also Lee et al. (2021)). The JULES outputs though, whilst spanning a similar range of reduced runoff, also show an increase in runoff when forced with some ESM patterns to an extent not shown by the CMIP6 models themselves. The reason for this is not known, but we note that in this case, future projections of Amazon runoff in PRIME show a wider spread than CMIP6 ensemble. The comparisons shown here illustrate that the PRIME framework gives a good indication of the CMIP6 ensemble spread for these known and very different scenarios to the training scenario. We show a range of different futures including overshoot and mitigation scenarios. This gives us some confidence that we can use this PRIME framework to provide a first look and assess some impacts from scenarios for which ESM simulations do not exist.

4 PRIME Impacts outputs

In this section, we present examples of how the PRIME framework can be used to assess climate impacts. Even though the SSP scenarios have been simulated by many ESMs in CMIP6, only a subset simulate the terrestrial carbon cycle (Arora et al., 2020), and very few simulate interactive dynamic vegetation (Pugh et al., 2018). Hence it is novel to show the possible spread of simulated carbon balance (represented by Net ecosystem productivity, NEP) and changes in tree fraction from a sample of percentiles that explore the full range of global temperature sensitivity.

In response to SSP1-2.6 (Figure 9) and SSP5-8.5 (not shown), terrestrial carbon storage increases almost everywhere in the multi-model mean with positive NEP (top row) especially evident in forested areas. The higher CO_2 concentration in the atmosphere drives enhanced vegetation photosynthesis (GPP; Fig. 8), which increases more than any loss from accelerated decomposition. This outweighs any detriment to vegetation productivity from changes in climate except in a few small regions such as southern Brazil. There is, though, significant spread across members with most regions showing potentially positive and negative NEP changes by 2100. This highlights the need for a probabilistic sampling of uncertainty not possible from a limited number of carbon-cycle ESMs. We note that this configuration of JULES does not include representation of fire which has been shown to improve GPP and vegetation distribution in ISIMIP2b simulations (Mathison et al., 2022). In addition, this configuration does not include permafrost carbon dynamics which could substantially alter this result as thawing of frozen

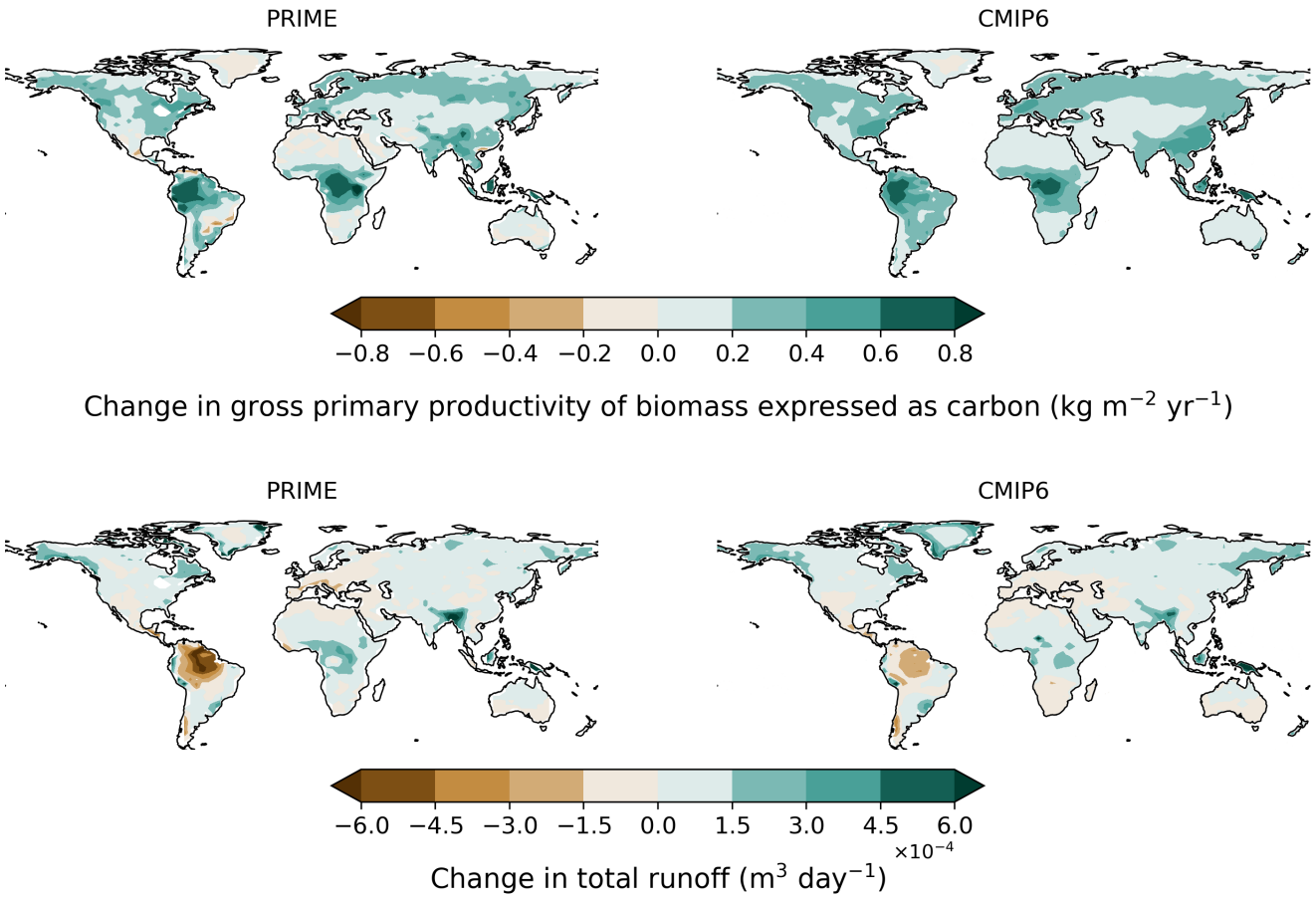

Figure 8. Maps comparing the multi-model mean projected end of century changes (2080–2100) for SSP1-2.6 in GPP (top) and runoff (bottom) from PRIME (left hand side) compared to CMIP6 (right hand side)

ground in the high latitudes is expected to mobilise large amounts of organic carbon (Chadburn et al., 2017; Burke et al., 2018; Varney et al., 2023). Both fire and permafrost carbon dynamics are part of planned future JULES configurations to be implemented in UKESM and therefore will be part of future versions of PRIME.

Accordingly, tree fraction increases in all regions (Fig. 9, bottom row). This is robust for India, Siberia and United States with relatively small spread compared to the mean signal of increased tree cover. In the Amazon region some ensemble members see a stabilisation and even beginning of loss of tree cover by 2100 as the effects of severe climate change counter the benefits due to elevated CO_2.

Jones et al. (2023) assessed CMIP6 carbon cycle projections against present day observations and also saw increases in biomass and total terrestrial carbon storage in all regions throughout the 21st century for SSP3-7.0. That study could not assess changes in vegetation cover as so few CMIP6 models represent dynamic vegetation. PRIME allows us to go beyond CMIP6 results to analyse impacts on vegetation dynamics and ecosystem composition as well as carbon balance.

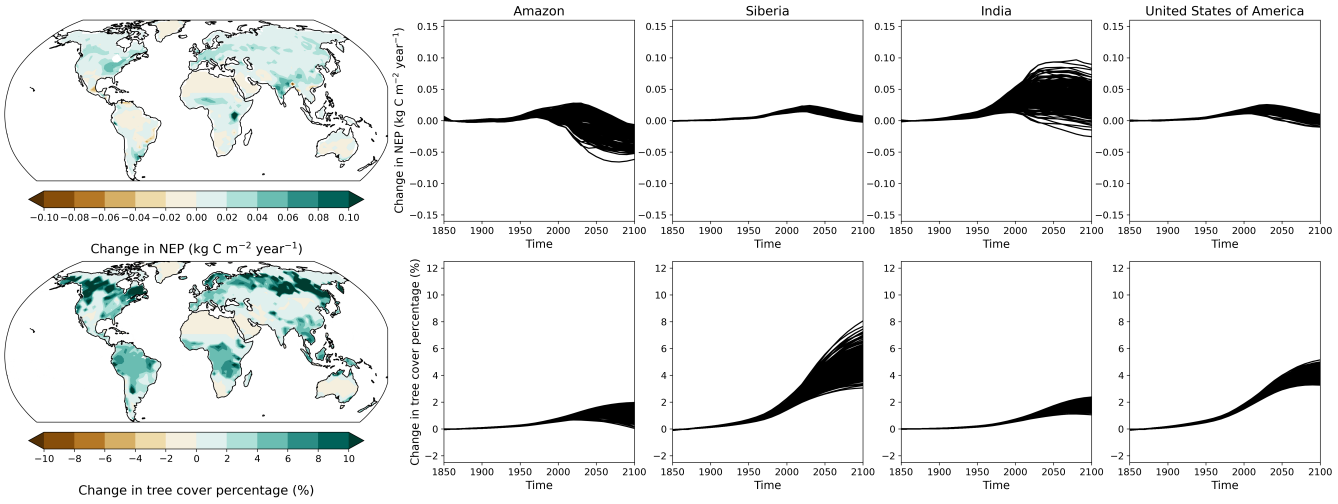

Figure 9. Maps of net ecosystem production (top) and tree fraction (bottom) with timeseries showing the median and uncertainty ranges for each study region: Amazon, Siberia, India and the USA (labelled) for SSP1-2.6 between 1850–2100.

5 Discussion, limitations and Conclusions

In this study, we document and evaluate the PRIME framework for the first time thereby providing capability for rapid probabilistic regional impacts assessments for any global emissions scenario to be produced in a fraction of the time it takes to run an ESM, being able to run hundreds of simulations in just a few days. We have shown that PRIME reproduces CMIP6 results for a range of SSP scenarios that have been simulated by full complexity ESMs, and in doing so demonstrated that the PRIME framework is fit for purpose.

The PRIME framework allows different sources of uncertainty to be quantified. FaIR provides a constrained probabilistic ensemble capturing the uncertainty in climate response, this is informed by the best available science from the IPCC, and can be easily refined or varied to sample any given range of global sensitivity. The advantages of an emulator like FaIR are its efficient run time and ability to provide projections for any emissions scenario outside of those run by ESMs. FaIR is very flexible and can be readily configured to run multiple scenarios, use multiple parameter sets or simulate idealised profiles as well as realistic scenarios and pathways.

The uncertainty from the full CMIP6 range of simulated patterns is provided through the construction of spatial patterns of change. It is widely accepted that the spatial patterns of change of many climate variables approximately scale with global temperature and are less dependent on a particular scenario or pathway (Mitchell, 2003; James et al., 2017; Tebaldi and Knutti, 2018; Arnell et al., 2019). As such, it is therefore possible to construct future projections of the spatial pattern of climate change given a pathway of global temperature change. This technique of "pattern scaling", when calibrated against a wide range of climate models, enables a rapid assessment of the range of climates for a given trajectory of global temperature. The limitations of the pattern scaling method and the potential for developing it are discussed in Section 5.1.

In this study we select our ensemble members mainly based on global temperature, however it is known that rising CO_2 concentration also has a direct effect on tropical circulation and precipitation patterns (Bony et al., 2013; Mitchell et al., 2016), which could affect the results shown here. In particular, (Mitchell et al., 2016) demonstrate that even if the global temperature stabilises, there is a continuing impact on the precipitation distribution. The joint distribution of the FaIR temperature and CO_2 concentrations being used in PRIME are shown in Section 3. This illustrates that although we capture the full temperature range through our selection of ensemble members based on global temperature, the higher CO_2 concentrations are not as well sampled. This is a limitation of the method we have chosen to select the ensemble members rather than a limitation of the PRIME framework, and will be explored in future iterations of the framework.

One of the main advantages of the PRIME framework is its flexibility, with the simple coupling between components lending itself to future couplings using other downstream models. For example, adding other models such as one for sea level rise or air quality to this framework would expand the scenario and climate output to get a rapid response of a broader range of impacts beyond land. Currently, we include just one land model, but other land models could be included in addition to JULES to capture the structural uncertainty in land models as well. It is also worth noting that the methods for downscaling to subdaily timescales in the form of the weather generator in JULES could benefit from more modern approaches which have not yet been investigated herein.

5.1 Limitations and opportunites for development

Pattern-scaling is a powerful methodology which has grown from its original intended purpose of providing a technique to allow extension of the relatively few computationally intensive simulations by ESMs to a broader remit. However there are two main limitations of this methodology. First, by definition, pattern scaling assumes the local and monthly changes in climate to be linear in global warming. Yet many studies show non-linearities in the climate response (King, 2019; Osborn et al., 2018; Chadwick and Good, 2013) and that the climate system may contain "tipping points" where strong non-linearity implies there may be future times when there are strong responses of Earth system components to relatively small additional increases in greenhouse gases (e.g., McKay et al., 2022). Linear scaling will not capture such rapid changes if they impact near-surface meteorology, although investigation of ESMs reveals relatively few instances of rapid change (Drijfhout et al., 2015). Although the use of pattern-scaling can currently only offer a linear interpretation of local and seasonal near-surface meteorological response to increasing greenhouse gases, the inclusion in PRIME of the full JULES land surface model does offer the opportunity to investigate in detail the risk of tipping points in land ecosystem response because JULES includes aspects of plant physiology and vegetation dynamics that are strongly nonlinear. A second limitation of pattern-scaling is that it does not resolve local land-atmosphere feedbacks and so will not capture in full the effects of major alterations to the land surface on near-surface meteorology. Such feedbacks may occur by the addition of new processes to land simulations that adjust substantially land-atmospheric exchanges of sensible or latent heat flux. Development of techniques to include such local feedbacks will form the basis of future research. Additionally, pattern scaling assumes that the patterns do not change with time and studies such as King et al. (2020) have shown changing spatial patterns of climate on long timescales as the system begins to equilibrate following an initial transient period. Yet experience with the MESMER tool has shown only

marginal improvement when additional predictors of patterns are added to global temperature, with the simple, conventional pattern scaling approach showing significant skill with errors typically much smaller than inter-model spread (Beusch et al., 2022).

There are alternate approaches to pattern-scaling such as the "time-shift" approach (Herger et al., 2015; Schleussner et al., 2013; King et al., 2017) which assumes that scenarios with equivalent global-mean temperatures exhibit similar regional climate changes. For example, a time period from an early transient high forcing simulation could be used to represent a climate sample for a lower forcing scenario. The advantage time shifting offers is that it avoids the linearity assumption and maintains physical consistency across multiple variables. However, there are parts of the climate system that are influenced by climate forcing rather than with global-mean temperature for example, Ceppi et al. (2018) show a poleward shift of the mid-latitude jets and Hadley cell edge in response to changes in forcing even before half the warming response has been realised. Furthermore, the history of the climate forcing as well as the balance of different forcing agents (which may evolve differently across different scenarios) also influences the regional climate change in scenarios with the same global mean temperature response.

Neither the approach of traditional pattern scaling or "time-shifting" is without limitations, with both providing useful capability. However, there is a need for fuller evaluation of pattern scaling approaches, including aspects such as winds, or snow cover where shifts may not scale with global T. An intercomparison of models like PRIME and MESMER would be a valuable addition to the literature. In addition, it would be useful to explore the use of multiple predictors such as land-sea contrast for more slowly evolving processes, along with CO_2 and aerosols for their direct effects. Ongoing research into land-use and direct regional biophysical effects will also be brought into subsequent versions of PRIME. For the future, PRIME is well positioned to exploit rapidly developing Artifical intelligence (AI) and machine learning (ML) methods, for example, Mansfield et al. (2023); Kitsios et al. (2023); Wilson Kemsley et al. (2024); Mansfield et al. (2020) to name a few. These offer substantial advances in deriving down-scaled and interpolated data which will be an area of development for PRIME.

5.2 Conclusions

Overall we have shown that PRIME is a flexible framework that runs quickly and produces reliable results for known scenarios. PRIME reproduces the climate response to a range of emissions scenarios (within the known limitations of the pattern-scaling approach) spanning global temperature in close agreement with IPCC assessments, capturing a range of 34 state-of-the-art Earth system models and simulating a range of land-surface outcomes and impacts. Although there are some variables that do not pattern scale as well as temperature, the performance for the key JULES input variables represents the range of CMIP6 models. This gives us confidence that PRIME will enable rapid and probabilistic assessment of novel scenarios, thereby providing a useful insight and the capability to quantify societally-relevant climate impacts.

6 Supplementary Information

Supplementary information provided in separate pdf file called 'Supplementary_for_PRIME_doc_paper.pdf'

Code availability. FaIR v1.6.2 is available from the Python Package Index at https://pypi.org/project/fair/1.6.2/, on GitHub at https://github.com/OMS-NetZero/FAIR/tree/v1.6.2, and at https://doi.org/10.5281/zenodo.4465032. Calibration data for FaIR v1.6.2 is available from https://doi.org/10.5281/zenodo.6601980. Climate patterns calculation code is available from ESMValTool https://zenodo.org/records/12654299.

Ticket has been opened to share the JULES code with reviewers of this manuscript.

Data availability. FaIR output used in PRIME is available from zenodo at this link: https://doi.org/10.5281/zenodo.10524337.
The ESMValTool patterns recipe linked above automatically downloads the CMIP6 data from ESGF https://esgf-node.llnl.gov/projects/esgf-llnl/, and calculates the patterns.
JULES output for the variables shown for each scenario are available from zenodo at this link: https://doi.org/10.5281/zenodo.10634291.

Author contributions. CM, EJB, CJ and CH came up with the original concept implemented here and contributed to running some of the individual components of the framework. GM created the patterns, EK completed the analysis of the individual components of the framework which make up many of the plots. CS provided expert knowledge on FaIR and CJ and AJW contributed scientific expertise particularly around the carbon cycle and JULES. LKG and LJV contributed to discussions and writing the manuscript. All were involved in bringing the ideas together and writing and commenting on the manuscript.DM contributed expertise at the revision stage on statistics and evaluation.

Competing interests. The authors can confirm they have no competing interests.

Acknowledgements. This work was supported by the Joint UK BEIS/Defra Met Office Hadley Centre Climate Programme (GA01101), the Newton Fund through the Met Office Climate Science for Service Partnership Brazil (CSSP Brazil), the Natural Environment Research Council (NE/T009381/1), and the European Union's Horizon 2020 research and innovation programme under Grant Agreement No 101003536 (ESM2025 - Earth System Models for the Future). N.J.S. acknowledges funding from the Research Council of Norway (project IMPOSE, grant 294930), as well as funding from the Norwegian Research Centre AS (NORCE). C.H. received support under national capability funding as part of the Natural Environment Research Council UK-SCAPE programme (award no. NE/R016429/1). R.M.V. was supported by the European Research Council's Climate–Carbon Interactions in the Current Century project (4C; grant no. 821003). C.S. was supported

by a NERC-IIASA collaborative research fellowship (NE/T009381/1) and the European Union's Horizon Europe research and innovation programme under Grant Agreement No 101081661 (WorldTrans).

References

Arnell, N. W., Lowe, J. A., Bernie, D., Nicholls, R. J., Brown, S., Challinor, A. J., and Osborn, T. J.: The global and regional impacts of climate change under representative concentration pathway forcings and shared socioeconomic pathway socioeconomic scenarios, Environmental Research Letters, 14, 084 046, https://doi.org/10.1088/1748-9326/ab35a6, 2019.

Arora, V. K., Katavouta, A., Williams, R. G., Jones, C. D., Brovkin, V., Friedlingstein, P., Schwinger, J., Bopp, L., Boucher, O., Cadule, P., Chamberlain, M. A., Christian, J. R., Delire, C., Fisher, R. A., Hajima, T., Ilyina, T., Joetzjer, E., Kawamiya, M., Koven, C. D., Krasting, J. P., Law, R. M., Lawrence, D. M., Lenton, A., Lindsay, K., Pongratz, J., Raddatz, T., Séférian, R., Tachiiri, K., Tjiputra, J. F., Wiltshire, A., Wu, T., and Ziehn, T.: Carbon–concentration and carbon–climate feedbacks in CMIP6 models and their comparison to CMIP5 models, Biogeosciences, 17, 4173–4222, https://doi.org/10.5194/bg-17-4173-2020, 2020.

Best, M. J., Pryor, M., Clark, D. B., Rooney, G. G., Essery, R. L. H., Menard, C. B., Edwards, J. M., Hendry, M. A., Porson, A., Gedney, N., Mercado, L. M., Sitch, S., Blyth, E., Boucher, O., Cox, P. M., Grimmond, C. S. B., and Harding, R. J.: The Joint UK Land Environment Simulator (JULES), model description - Part 1: Energy and water fluxes, GEOSCIENTIFIC MODEL DEVELOPMENT, 4, 677–699, https://doi.org/10.5194/gmd-4-677-2011, 2011.

Beusch, L., Gudmundsson, L., and Seneviratne, S. I.: Emulating Earth system model temperatures with MESMER: from global mean temperature trajectories to grid-point-level realizations on land, Earth System Dynamics, 11, 139–159, https://doi.org/10.5194/esd-11-139-2020, 2020.

Beusch, L., Nicholls, Z., Gudmundsson, L., Hauser, M., Meinshausen, M., and Seneviratne, S. I.: From emission scenarios to spatially resolved projections with a chain of computationally efficient emulators: coupling of MAGICC (v7.5.1) and MESMER (v0.8.3), Geoscientific Model Development, 15, 2085–2103, https://doi.org/10.5194/gmd-15-2085-2022, 2022.

Bony, S., Bellon, G., Klocke, D., Sherwood, S., Fermepin, S., and Denvil, S.: Robust direct effect of carbon dioxide on tropical circulation and regional precipitation, Nature Geoscience, https://doi.org/10.1038/ngeo1799, 2013.

Burke, E. J., Ekici, A., Huang, Y., Chadburn, S. E., Huntingford, C., Ciais, P., Friedlingstein, P., Peng, S., and Krinner, G.: Quantifying uncertainties of permafrost carbon–climate feedbacks, Biogeosciences, 14, 3051–3066, 2017.

Burke, E. J., Chadburn, S. E., Huntingford, C., and Jones, C. D.: CO2 loss by permafrost thawing implies additional emissions reductions to limit warming to 1.5 or 2 °C, Environmental Research Letters, 13, 024 024, https://doi.org/10.1088/1748-9326/aaa138, 2018.

Burton, C., Betts, R. A., Jones, C. D., Feldpausch, T. R., Cardoso, M., and Anderson, L. O.: El Niño Driven Changes in Global Fire 2015/16, Frontiers in Earth Science, 8, https://doi.org/10.3389/feart.2020.00199, 2020.

Ceppi, P., Zappa, G., Shepherd, T. G., and Gregory, J. M.: Fast and slow components of the extratropical atmospheric circulation response to CO2 forcing., Journal of Climate, https://doi.org/https://doi.org/10.1175/JCLI-D-17-0323.1, 2018.

Chadburn, S., Burke, E., Cox, P., Friedlingstein, P., Hugelius, G., and Westermann, S.: An observation-based constraint on permafrost loss as a function of global warming, Nature Climate Change, 7, 340–344, https://doi.org/10.1038/nclimate3262, 2017.

Chadwick, R. and Good, P.: Understanding nonlinear tropical precipitation responses to CO2 forcing, Geophys. Res. Lett., https://doi.org/https://doi.org/10.1002/grl.50932, 2013.

Clark, D. B., Mercado, L. M., Sitch, S., Jones, C. D., Gedney, N., Best, M. J., Pryor, M., Rooney, G. G., Essery, R. L. H., Blyth, E., Boucher, O., Harding, R. J., Huntingford, C., and Cox, P. M.: The Joint UK Land Environment Simulator (JULES), model description - Part 2: Carbon fluxes and vegetation dynamics, GEOSCIENTIFIC MODEL DEVELOPMENT, 4, 701–722, https://doi.org/10.5194/gmd-4-701-2011, 2011.

Collins, M., Knutti, R., Arblaster, J., Dufresne, J.-L., Fichefet, T., Friedlingstein, P., Gao, X., Gutowski, W., Johns, T., Krinner, G., Shongwe, M., Tebaldi, C., Weaver, A., and Wehner, M.: Long-term Climate Change: Projections, Commitments and Irreversibility, in: Climate Change 2013: The Physical Science Basis. Contribution of Working Group I to the Fifth Assessment Report of the Intergovernmental Panel on Climate Change, edited by Stocker, T., Qin, D., Plattner, G.-K., Tignor, M., Allen, S., Boschung, J., Nauels, A., Xia, Y., Bex, V., and Midgley, P., book section 12, p. 1029–1136, Cambridge University Press, Cambridge, United Kingdom and New York, NY, USA, https://doi.org/10.1017/CBO9781107415324.024, 2013.

Collins, W., Bellouin, N., Doutriaux-Boucher, M., Gedney, N., Halloran, P., Hinton, T., Hughes, J., Jones, C., Joshi, M., Liddicoat, S., Martin, G., O'Connor, F., Rae, J., Senior, C., Sitch, S., Totterdell, I., Wiltshire, A., and Woodward, S.: Development and evaluation of an Earth System model, HADGEM2, Geoscientific Model Development, 4, 1051–1075, https://doi.org/10.5194/gmd-4-1051-2011, 2011.

Cox, P. M.: Description of the TRIFFID dynamic global vegetation model, Tech. rep., https://digital.nmla.metoffice.gov.uk/IO_cc8f146a-d524-4243-88fc-e3a3bcd782e7/, 2001.

Drijfhout, S., Bathiany, S., Beaulieu, C., Brovkin, V., Claussen, M., Huntingford, C., Scheffer, M., Sgubin, G., and Swingedouw, D.: Catalogue of abrupt shifts in Intergovernmental Panel on Climate Change climate models, PROCEEDINGS OF THE NATIONAL ACADEMY OF SCIENCES OF THE UNITED STATES OF AMERICA, 112, E5777–E5786, https://doi.org/10.1073/pnas.1511451112, 2015.

Dvorak, M., Armour, K., Frierson, D., Proistosescu, C., Baker, M., and Smith, C.: Estimating the timing of geophysical commitment to 1.5 and 2.0° C of global warming, Nature Climate Change, 12, 547–552, 2022.

Eyring, V., Bony, S., Meehl, G. A., Senior, C. A., Stevens, B., Stouffer, R. J., and Taylor, K. E.: Overview of the Coupled Model Intercomparison Project Phase 6 (CMIP6) experimental design and organization, Geoscientific Model Development, 9, 1937–1958, https://doi.org/10.5194/gmd-9-1937-2016, 2016.

Forster, P., Storelvmo, T., Armour, K., Collins, W., Dufresne, J. L., Frame, D., Lunt, D. J., Mauritsen, T., Palmer, M. D., Watanabe, M., Wild, M., and Zhang, H.: The Earth's Energy Budget, Climate Feedbacks, and Climate Sensitivity, in: Climate Change 2021: The Physical Science Basis. Contribution of Working Group I to the Sixth Assessment Report of the Intergovernmental Panel on Climate Change, edited by Masson-Delmotte, V., Zhai, P., Pirani, A., Connors, S. L., Péan, C., Berger, S., Caud, N., Chen, Y., Goldfarb, L., Gomis, M. I., Huang, M., Leitzell, K., Lonnoy, E., Matthews, J. B. R., Maycock, T. K., Waterfield, T., Yelekçi, O., Yu, R., and Zhou, B., Cambridge University Press, https://www.ipcc.ch/report/ar6/wg1/downloads/report/IPCC_AR6_WGI_Chapter_07.pdf, 2021.

Forster, P. M., Smith, C. J., Walsh, T., Lamb, W. F., Lamboll, R., Hauser, M., Ribes, A., Rosen, D., Gillett, N., Palmer, M. D., Rogelj, J., von Schuckmann, K., Seneviratne, S. I., Trewin, B., Zhang, X., Allen, M., Andrew, R., Birt, A., Borger, A., Boyer, T., Broersma, J. A., Cheng, L., Dentener, F., Friedlingstein, P., Gutiérrez, J. M., Gütschow, J., Hall, B., Ishii, M., Jenkins, S., Lan, X., Lee, J.-Y., Morice, C., Kadow, C., Kennedy, J., Killick, R., Minx, J. C., Naik, V., Peters, G. P., Pirani, A., Pongratz, J., Schleussner, C.-F., Szopa, S., Thorne, P., Rohde, R., Rojas Corradi, M., Schumacher, D., Vose, R., Zickfeld, K., Masson-Delmotte, V., and Zhai, P.: Indicators of Global Climate Change 2022: annual update of large-scale indicators of the state of the climate system and human influence, Earth System Science Data, 15, 2295–2327, https://doi.org/10.5194/essd-15-2295-2023, 2023.

Frieler, K., Lange, S., Piontek, F., Reyer, C. P. O., Schewe, J., Warszawski, L., Zhao, F., Chini, L., Denvil, S., Emanuel, K., Geiger, T., Halladay, K., Hurtt, G., Mengel, M., Murakami, D., Ostberg, S., Popp, A., Riva, R., Stevanovic, M., Suzuki, T., Volkholz, J., Burke, E., Ciais, P., Ebi, K., Eddy, T. D., Elliott, J., Galbraith, E., Gosling, S. N., Hattermann, F., Hickler, T., Hinkel, J., Hof, C., Huber, V., Jägermeyr, J., Krysanova, V., Marcé, R., Müller Schmied, H., Mouratiadou, I., Pierson, D., Tittensor, D. P., Vautard, R., van Vliet, M., Biber, M. F., Betts, R. A., Bodirsky, B. L., Deryng, D., Frolking, S., Jones, C. D., Lotze, H. K., Lotze-Campen, H., Sahajpal, R., Thonicke, K., Tian, H., and

Yamagata, Y.: Assessing the impacts of 1.5°C global warming – simulation protocol of the Inter-Sectoral Impact Model Intercomparison Project (ISIMIP2b), Geoscientific Model Development, 10, 4321–4345, https://doi.org/10.5194/gmd-10-4321-2017, 2017.

Frieler, K., Volkholz, J., Lange, S., Schewe, J., Mengel, M., Rivas López, M. d. R., Otto, C., Reyer, C. P., Karger, D. N., Malle, J. T., et al.: Scenario set-up and forcing data for impact model evaluation and impact attribution within the third round of the Inter-Sectoral Model Intercomparison Project (ISIMIP3a), EGUsphere, pp. 1–83, 2023.

Goodwin, P., Leduc, M., Partanen, A.-I., Matthews, H. D., and Rogers, A.: A computationally efficient method for probabilistic local warming projections constrained by history matching and pattern scaling, demonstrated by WASP–LGRTC-1.0, Geoscientific Model Development, 13, 5389–5399, https://doi.org/10.5194/gmd-13-5389-2020, 2020.

Herger, N., Sanderson, B. M., and Knutti, R.: .: Improved pattern scaling approaches for the use in climate impact studies, Geophysical Research Letters, 42, 3486–3494, https://doi.org/3486–3494, doi:10.1002/2015GL063569, 2015.

Huntingford, C. and Cox, P.: An analogue model to derive additional climate change scenarios from existing GCM simulations, CLIMATE DYNAMICS, 16, 575–586, https://doi.org/10.1007/s003820000067, 2000.

Huntingford, C., Booth, B. B. B., Sitch, S., Gedney, N., Lowe, J. A., Liddicoat, S. K., Mercado, L. M., Best, M. J., Weedon, G. P., Fisher, R. A., Lomas, M. R., Good, P., Zelazowski, P., Everitt, A. C., Spessa, A. C., and Jones, C. D.: IMOGEN: an intermediate complexity model to evaluate terrestrial impacts of a changing climate, GEOSCIENTIFIC MODEL DEVELOPMENT, 3, 679–687, https://doi.org/10.5194/gmd-3-679-2010, 2010.

IPCC: Climate Change 2021: The Physical Science Basis. Contribution of Working Group I to the Sixth Assessment Report of the Intergovernmental Panel on Climate Change, Cambridge University Press, Cambridge, UK and New York, NY, USA, https://doi.org/10.1017/9781009157896, 2021.

IPCC: Climate Change 2022: Mitigation of Climate Change. Contribution of Working Group III to the Sixth Assessment Report of the Intergovernmental Panel on Climate Change, Cambridge University Press, Cambridge, UK and New York, NY, USA, https://doi.org/10.1017/9781009157926, 2022.

James, R., Washington, R., Schleussner, C.-F., Rogelj, J., and Conway, D.: Characterizing half-a-degree difference: a review of methods for identifying regional climate responses to global warming targets, WIREs Climate Change, 8, e457, https://doi.org/https://doi.org/10.1002/wcc.457, 2017.

Jones, C. D., Hughes, J. K., Bellouin, N., Hardiman, S. C., Jones, G. S., Knight, J., Liddicoat, S., O'Connor, F. M., Andres, R. J., Bell, C., Boo, K.-O., Bozzo, A., Butchart, N., Cadule, P., Corbin, K. D., Doutriaux-Boucher, M., Friedlingstein, P., Gornall, J., Gray, L., Halloran, P. R., Hurtt, G., Ingram, W. J., Lamarque, J.-F., Law, R. M., Meinshausen, M., Osprey, S., Palin, E. J., Parsons Chini, L., Raddatz, T., Sanderson, M. G., Sellar, A. A., Schurer, A., Valdes, P., Wood, N., Woodward, S., Yoshioka, M., and Zerroukat, M.: The HadGEM2-ES implementation of CMIP5 centennial simulations, Geoscientific Model Development, 4, 543–570, https://doi.org/10.5194/gmd-4-543-2011, 2011.

Jones, C. D., Ziehn, T., Anand, J., Bastos, A., Burke, E., Canadell, J. G., Cardoso, M., Ernst, Y., Jain, A. K., Jeong, S., Keller, E. D., Kondo, M., Lauerwald, R., Lin, T.-S., Murray-Tortarolo, G., Nabuurs, G.-J., O'Sullivan, M., Poulter, B., Qin, X., von Randow, C., Sanches, M., Schepaschenko, D., Shvidenko, A., Smallman, T. L., Tian, H., Villalobos, Y., Wang, X., and Yun, J.: RECCAP2 Future Component: Consistency and Potential for Regional Assessment to Constrain Global Projections, AGU Advances, 4, e2023AV001 024, https://doi.org/https://doi.org/10.1029/2023AV001024, e2023AV001024 2023AV001024, 2023.

King, A., Karoly, D., and Henley, B.: Australian climate extremes at 1.5°C and 2°C of global warming., Nat. Clim. Change, 2017.

King, A. D.: The drivers of nonlinear local temperature change under global warming, Environ. Res. Lett., 14, 064 005, https://doi.org/10.1088/1748-9326/ab1976, 2019.

King, A. D., Lane, T. P., Henley, B. J., and Brown, J. R.: Global and regional impacts differ between transient and equilibrium warmer worlds, Nature Climate Change, 10, 42–47, 2020.

Kitsios, V., O'Kane, T. J., and Newth, D.: A machine learning approach to rapidly project climate responses under a multitude of net-zero emission pathways, Nature Communications Earth & Environment, https://doi.org/10.1038/s43247-023-01011-0, 2023.

Kravitz, B., Lynch, C., Hartin, C., and Bond-Lamberty, B.: Exploring precipitation pattern scaling methodologies and robustness among CMIP5 models, Geoscientific Model Development, 10, 1889–1902, https://doi.org/10.5194/gmd-10-1889-2017, 2017.

Leach, N. J., Jenkins, S., Nicholls, Z., Smith, C. J., Lynch, J., Cain, M., Walsh, T., Wu, B., Tsutsui, J., and Allen, M. R.: FaIRv2.0.0: A generalized impulse response model for climate uncertainty and future scenario exploration, Geoscientific Model Development, 14, 3007–3036, https://doi.org/10.5194/gmd-14-3007-2021, 2021.

Lee, J.-Y., Marotzke, J., Bala, G., Cao, L., Corti, S., Dunne, J., Engelbrecht, F., Fischer, E., Fyfe, J., Jones, C., Maycock, A., Mutemi, J., Ndiaye, O., Panickal, S., and Zhou, T.: Future Global Climate: Scenario-Based Projections and Near-Term Information, in: Climate Change 2021: The Physical Science Basis. Contribution of Working Group I to the Sixth Assessment Report of the Intergovernmental Panel on Climate Change, edited by Masson-Delmotte, V., Zhai, P., Pirani, A., Connors, S. L., Péan, C., Berger, S., Caud, N., Chen, Y., Goldfarb, L., Gomis, M. I., Huang, M., Leitzell, K., Lonnoy, E., Matthews, J. B. R., Maycock, T. K., Waterfield, T., Yelekçi, O., Yu, R., and Zhou, B., book section 4, Cambridge University Press, Cambridge, UK and New York, NY, USA, https://doi.org/10.1017/9781009157896.006, 2021.

Mansfield, L., Nowack, P., Kasoar, M., Everitt, R., Collins, W. J., and Voulgarakis, A.: Predicting global patterns of long-term climate change from short-term simulations using machine learning., npj,Cliamte and Atmospheric Science, https://doi.org/https://doi.org/10.1038/s41612-020-00148-5, 2020.

Mansfield, L. A., Gupta, A., Burnett, A. C., Green, B., Wilka, C., and Sheshadri, A.: Updates on Model Hierarchies for Understanding and Simulating the Climate System: A Focus on Data-Informed Methods and Climate Change Impacts, Journal of Advances in Modeling Earth Systems, 15, e2023MS003 715, https://doi.org/https://doi.org/10.1029/2023MS003715, e2023MS003715 2023MS003715, 2023.

Mathison, C., Burke, E., Hartley, A. J., Kelley, D. I., Burton, C., Robertson, E., Gedney, N., Williams, K., Wiltshire, A., Ellis, R. J., et al.: Description and Evaluation of the JULES-ES setup for ISIMIP2b, EGUsphere, 2022, 1–24, 2022.

McKay, D. I. A., Staal, A., Abrams, J. F., Winkelmann, R., Sakschewski, B., Loriani, S., Fetzer, I., Cornell, S. E., Rockström, J., and Lenton, T. M.: Exceeding 1.5°C global warming could trigger multiple climate tipping points, Science, 377, eabn7950, 2022.

Mercado, L. M., Bellouin, N., Sitch, S., Boucher, O., Huntingford, C., Wild, M., and Cox, P. M.: Impact of changes in diffuse radiation on the global land carbon sink, NATURE, 458, 1014–U87, https://doi.org/10.1038/nature07949, 2009.

Mitchell, D., James, R., Forster, P. M., Betts, R. A., Shiogama, H., and Allen, M.: Realizing the impacts of a 1.5 °C warmer world, Nature Climate Change, https://doi.org/10.1038/nclimate3055, 2016.

Mitchell, T. D.: Pattern scaling: an examination of the accuracy of the technique for describing future climates, Climatic change, 60, 217–242, 2003.

Nath, S., Lejeune, Q., Beusch, L., Seneviratne, S. I., and Schleussner, C.-F.: MESMER-M: an Earth system model emulator for spatially resolved monthly temperature, Earth System Dynamics, 13, 851–877, https://doi.org/10.5194/esd-13-851-2022, 2022.

Nicholls, Z., Meinshausen, M., Lewis, J., Corradi, M. R., Dorheim, K., Gasser, T., Gieseke, R., Hope, A. P., Leach, N. J., McBride, L. A., Quilcaille, Y., Rogelj, J., Salawitch, R. J., Samset, B. H., Sandstad, M., Shiklomanov, A., Skeie, R. B., Smith,

C. J., Smith, S. J., Su, X., Tsutsui, J., Vega-Westhoff, B., and Woodard, D. L.: Reduced Complexity Model Intercomparison Project Phase 2: Synthesizing Earth System Knowledge for Probabilistic Climate Projections, Earth's Future, 9, e2020EF001 900, https://doi.org/https://doi.org/10.1029/2020EF001900, e2020EF001900 2020EF001900, 2021.

Nicholls, Z. R. J., Meinshausen, M., Lewis, J., Gieseke, R., Dommenget, D., Dorheim, K., Fan, C.-S., Fuglestvedt, J. S., Gasser, T., Golüke, U., Goodwin, P., Hartin, C., Hope, A. P., Kriegler, E., Leach, N. J., Marchegiani, D., McBride, L. A., Quilcaille, Y., Rogelj, J., Salawitch, R. J., Samset, B. H., Sandstad, M., Shiklomanov, A. N., Skeie, R. B., Smith, C. J., Smith, S., Tanaka, K., Tsutsui, J., and Xie, Z.: Reduced Complexity Model Intercomparison Project Phase 1: introduction and evaluation of global-mean temperature response, Geoscientific Model Development, 13, 5175–5190, https://doi.org/10.5194/gmd-13-5175-2020, 2020.

Osborn, T. J., Wallace, C. J., Lowe, J. A., and Bernie, D.: Performance of pattern-scaled climate projections under high-end warming. Part I: Surface air temperature over land, J. Climate, https://doi.org/https://doi.org/10.1175/JCLI-D-17-0780.1, 2018.

Pugh, T. A. M., Jones, C. D., Huntingford, C., Burton, C., Arneth, A., Brovkin, V., Ciais, P., Lomas, M., Robertson, E., Piao, S. L., and Sitch, S.: A Large Committed Long-Term Sink of Carbon due to Vegetation Dynamics, Earth's Future, 6, 1413–1432, https://doi.org/https://doi.org/10.1029/2018EF000935, 2018.

Pörtner, H. O., Roberts, D. C., Tignor, M., Poloczanska, E. S., Mintenbeck, K., Alegría, A., Craig, M., Langsdorf, S., Löschke, S., Möller, V., Okem, A., and Rama, B., eds.: Full report, p. In Press, Cambridge University Press, Cambridge, UK, in Press, 2022.

Quilcaille, Y., Gudmundsson, L., Beusch, L., Hauser, M., and Seneviratne, S. I.: Showcasing MESMER-X: Spatially Resolved Emulation of Annual Maximum Temperatures of Earth System Models, Geophysical Research Letters, 49, e2022GL099 012, https://doi.org/https://doi.org/10.1029/2022GL099012, e2022GL099012 2022GL099012, 2022.

Riahi, K., Schaeffer, R., Arango, J., Calvin, K., Guivarch, C., Hasegawa, T., Jiang, K., Kriegler, E., Matthews, R., Peters, G. P., Rao, A., Robertson, S., Sebbit, A. M., Steinberger, J., Tavoni, M., and Vuuren, D. P. V.: Mitigation pathways compatible with long-term goals., in: IPCC, 2022: Climate Change 2022: Mitigation of Climate Change. Contribution of Working Group III to the Sixth Assessment Report of the Intergovernmental Panel on Climate Change, edited by Shukla, P. R., Skea, J., Slade, R., Khourdajie, A. A., van Diemen, R., McCollum, D., Pathak, M., Some, S., Vyas, P., Fradera, R., Belkacemi, M., Hasija, A., Lisboa, G., Luz, S., and Malley, J., Cambridge University Press, https://doi.org/10.1017/9781009157926.005, 2022.

Richters, O., Bertram, C., Kriegler, E., Al Khourdajie, A., Cui, R., Edmonds, J., Hackstock, P., Holland, D., Hurst, I., Kikstra, J., Lewis, J., Liadze, I., Meinshausen, M., Min, J., Nicholls, Z., Piontek, F., Sauer, I., Sferra, F., Sanchez Juanino, P., van Ruijven, B., Weigmann, P., Yu, S., Zhao, A., and Zwerling, M.: NGFS Climate Scenarios Data Set, https://doi.org/10.5281/zenodo.7198430, This work was made possible by grants from Bloomberg Philanthropies and ClimateWorks Foundation., 2022.

Rogelj, J., Shindell, D., Jiang, K., Fifita, S., Forster, P., Ginzburg, V., Handa, C., Kheshgi, H., Kobayashi, S., Kriegler, E., Mundaca, L., Séférian, R., and Vilariño, M. V.: Mitigation Pathways Compatible with 1.5°C in the Context of Sustainable Development, in: Global Warming of 1.5°C: An IPCC Special Report on the impacts of global warming of 1.5°C above pre-industrial levels and related global greenhouse gas emission pathways, in the context of strengthening the global response to the threat of climate change, sustainable development, and efforts to eradicate poverty, edited by Masson-Delmotte, V., Zhai, P., Pörtner, H.-O., Roberts, D., Skea, J., Shukla, P. R., Pirani, A., Moufouma-Okia, W., Péan, C., Pidcock, R., Connors, S., Matthews, J. B. R., Chen, Y., Zhou, X., Gomis, M. I., Lonnoy, E., Maycock, T., Tignor, M., and Waterfield, T., World Meteorological Organization, Geneva, Switzerland, https://www.ipcc.ch/sr15/, 2018.

Schleussner, C. F., Lissner, T. K., Fischer, E. M., Wohland, J., Perrette, M., Golly, A., Rogelj, J., Chiders, K., Schewe, J., Frieler, K., Mengal, M., Hare, W., and Schaeffer, M.: Differential climate impacts for policy-relevant limits to global warming: The case of 1.5 °C and 2 °C., Earth System Dynamics, https://doi.org/https://doi.org/10.5194/esd-7-327-2016, 2013.

Sellar, A. A., Jones, C. G., Mulcahy, J. P., Tang, Y., Yool, A., Wiltshire, A., O'connor, F. M., Stringer, M., Hill, R., Palmieri, J., et al.: UKESM1: Description and evaluation of the UK Earth System Model, Journal of Advances in Modeling Earth Systems, 11, 4513–4558, 2019.

Smith, C.: FaIR v1.6.2 calibrated and constrained parameter set, https://doi.org/10.5281/zenodo.6601980, 2022.

Smith, C., Cummins, D. P., Fredriksen, H.-B., Nicholls, Z., Meinshausen, M., Allen, M., Jenkins, S., Leach, N., Mathison, C., and Partanen, A.-I.: fair-calibrate v1.4.1: calibration, constraining and validation of the FaIR simple climate model for reliable future climate projections, EGUsphere, 2024, 1–36, https://doi.org/10.5194/egusphere-2024-708, 2024.

Smith, C. J., Forster, P. M., Allen, M., Leach, N., Millar, R. J., Passerello, G. A., and Regayre, L. A.: FAIR v1.3: a simple emissions-based impulse response and carbon cycle model, Geoscientific Model Development, 11, 2273–2297, https://doi.org/10.5194/gmd-11-2273-2018, 2018.

Smith, C. J., Nicholls, Z. R. J., Armour, K., Collins, W., Forster, P., Meinshausen, M., Palmer, M. D., and Watanabe, M.: The Earth's Energy Budget, Climate Feedbacks, and Climate Sensitivity Supplementary Material, in: Climate Change 2021: The Physical Science Basis. Contribution of Working Group I to the Sixth Assessment Report of the Intergovernmental Panel on Climate Change, edited by Masson-Delmotte, V., Zhai, P., Pirani, A., Connors, S. L., Péan, C., Berger, S., Caud, N., Chen, Y., Goldfarb, L., Gomis, M. I., Huang, M., Leitzell, K., Lonnoy, E., Matthews, J. B. R., Maycock, T. K., Waterfield, T., Yelekçi, O., Yu, R., and Zhou, B., Cambridge University Press, https://www.ipcc.ch/report/ar6/wg1/downloads/report/IPCC_AR6_WGI_Chapter_07_Supplementary_Material.pdf, 2021.

Smith, C. J., Khourdajie, A. A., Yang, P., and Folini, D.: Climate uncertainty impacts on optimal mitigation pathways and social cost of carbon, Environmental Research Letters, 18, 094 024, https://doi.org/10.1088/1748-9326/acedc6, 2023.

Stanhill, G. and Cohen, S.: Global dimming: a review of the evidence for a widespread and significant reduction in global radiation with discussion of its probable causes and possible agricultural consequences, Agricultural and Forest Meteorology, 107, 255–278, https://doi.org/https://doi.org/10.1016/S0168-1923(00)00241-0, 2001.

Taylor, K. E., Stouffer, R. J., and Meehl, G. A.: An Overview of CMIP5 and the Experiment Design, Bulletin of the American Meteorological Society, 93, 485–498, https://doi.org/https://doi.org/10.1175/BAMS-D-11-00094.1, 2012.

Tebaldi, C. and Arblaster, J. M.: Pattern scaling: Its strengths and limitations, and an update on the latest model simulations, Climatic Change, 122, 459–471, 2014.

Tebaldi, C. and Knutti, R.: Evaluating the accuracy of climate change pattern emulation for low warming targets, Environmental Research Letters, 13, 055 006, https://doi.org/10.1088/1748-9326/aabef2, 2018.

Tebaldi, C., Snyder, A., and Dorheim, K.: STITCHES: creating new scenarios of climate model output by stitching together pieces of existing simulations, Earth System Dynamics, 13, 1557–1609, https://doi.org/10.5194/esd-13-1557-2022, 2022.

van Vuuren, D. P., Lowe, J., Stehfest, E., Gohar, L., Hof, A. F., Hope, C., Warren, R., Meinshausen, M., and Plattner, G.-K.: How well do integrated assessment models simulate climate change?, Climatic Change, 104, 255–285, https://doi.org/10.1007/s10584-009-9764-2, 2011.

Varney, R. M., Chadburn, S. E., Burke, E. J., Jones, S., Wiltshire, A. J., and Cox, P. M.: Simulated responses of soil carbon to climate change in CMIP6 Earth system models: the role of false priming, Biogeosciences, 20, 3767–3790, 2023.

Wang, Z., Zhang, M., Wang, L., and Qin, W.: A comprehensive research on the global all-sky surface solar radiation and its driving factors during 1980–2019., Atmos Research, 265, https://doi.org/https://doi.org/10.1016/j.atmosres.2021.105870, 2022.

Warszawski, L., Friend, A., Ostberg, S., Frieler, K., Lucht, W., Schaphoff, S., Beerling, D., Cadule, P., Ciais, P., Clark, D. B., Kahana, R., Ito, A., Keribin, R., Kleidon, A., Lomas, M., Nishina, K., Pavlick, R., Rademacher, T. T., Buechner, M., Piontek, F., Schewe, J., Serdeczny,

O., and Schellnhuber, H. J.: A multi-model analysis of risk of ecosystem shifts under climate change, Environmental Research Letters, 8, 044 018, http://stacks.iop.org/1748-9326/8/i=4/a=044018, 2013.

Warszawski, L., Frieler, K., Huber, V., Piontek, F., Serdeczny, O., and Schewe, J.: The Inter-Sectoral Impact Model Intercomparison Project (ISI-MIP): Project framework, Proceedings of the National Academy of Sciences, 111, 3228–3232, https://doi.org/10.1073/pnas.1312330110, 2014.

Wells, C. D., Jackson, L. S., Maycock, A. C., and Forster, P. M.: Understanding pattern scaling errors across a range of emissions pathways, Earth System Dynamics, 14, 817–834, https://doi.org/10.5194/esd-14-817-2023, 2023.

Williams, K. and Clark, D.: Hadley Centre Technical Note 96 Disaggregation of daily data in JULES, Tech. rep., Met Office, 2014.

Wilson Kemsley, S., Osborn, T., Dorling, S., and Wallace, C.: Pattern scaling the parameters of a Markov-Chain gamma-distribution daily precipitation generator, International Journal of Climatology, 44, 144–159, https://doi.org/10.1002/joc.8320, 2024.

Wiltshire, A. J., Burke, E. J., Chadburn, S. E., Jones, C. D., Cox, P. M., Davies-Barnard, T., Friedlingstein, P., Harper, A. B., Liddicoat, S., Sitch, S., et al.: JULES-CN: a coupled terrestrial carbon–nitrogen scheme (JULES vn5. 1), Geoscientific Model Development, 14, 2161–2186, 2021.

Zelazowski, P., Huntingford, C., Mercado, L. M., and Schaller, N.: Climate pattern-scaling set for an ensemble of 22 GCMs – adding uncertainty to the IMOGEN version 2.0 impact system, Geoscientific Model Development, 11, 541–560, https://doi.org/10.5194/gmd-11-541-2018, 2018.